Materials Research Bulletin 182 (2025) 113114

Contents lists available at ScienceDirect

Materials Research Bulletin

journal homepage: www.elsevier.com/locate/matresbu

Research Papers

# Stability enhancement of molybdenum modified rutile – carbon composite supported platinum electrocatalysts by reductive pretreatment: Surface characteristics and advanced electrocatalytic properties

Cristina Silva [a,b], Irina Borbáth [a], Erzsébet Dodony [c], Dániel Olasz [c], György Sáfrán [c], Ágnes Szegedi [a], Kristóf Zelenka [a], András Tompos [a,*], Zoltán Pászti [a]

[a] Institute of Materials and Environmental Chemistry, HUN-REN Research Centre for Natural Sciences, Magyar Tudósok körútja 2, Budapest H-1117, Hungary
[b] Department of Physical Chemistry and Materials Science, Faculty of Chemical Technology and Biotechnology, Budapest University of Technology and Economics, Műegyetem rakpart. 3., Budapest H-1111, Hungary
[c] Institute for Technical Physics and Materials Science, HUN-REN Centre for Energy Research, Konkoly-Thege Miklós út 29-33, Budapest H-1121, Hungary

ARTICLE INFO

*Keywords:*
A: composites
A: nanostructures
B: sol-gel chemistry
D: catalytic properties
D: electrochemical properties

ABSTRACT

Development of strong metal-support interaction (SMSI) and its influence on the catalytic performance of the Pt/$Ti_{0.8}Mo_{0.2}O_2$-C system, a representative of the mixed oxide-carbon composite supported Pt electrocatalyst family, were investigated. Structural, surface chemical and electrochemical properties of the *as-prepared* Pt/$Ti_{0.8}Mo_{0.2}O_2$-C catalyst and its counterparts reduced in the 150–450 °C temperature range were compared. TEM elemental mapping confirmed the widespread formation of Pt-oxide-C triple junctions in all catalysts. XPS revealed electronic interaction between the Pt particles and the oxide both in the *as-prepared* and the reduced catalysts, moreover, demonstrated that transport of Mo to the surface of Pt is initiated by reduction in the 150–250 °C range. Electrochemical measurements pointed out the durability of these Pt-bound Mo species, which also enhance the oxygen reduction activity of the catalyst. Based on the results of 10,000-cycle stability tests, reductive pretreatment between 250–350 °C is recommended for enhancing the properties of Pt/$Ti_{0.8}Mo_{0.2}O_2$-C catalysts by SMSI.

## 1. Introduction

### 1.1. Oxide and oxide-carbon composite supports for Pt electrocatalysts

Catalyst stability is a key issue in heterogeneous catalysis; it is as important in determining the performance of a catalyst than its activity or selectivity. In particular, special emphasis is placed on long-term stability/reusability in industrial processes [1]. While deactivation mechanisms of catalysts used in gas phase thermally activated processes were relatively well understood, stability concerns of catalysts working in electrochemical reactions under aqueous environments were identified as pressing issues only in the last one or two decades, mostly with the advent of interest towards electrochemical energy conversion devices.

Among these devices, fuel cells generate electrical energy from the chemical energy released during oxidation of hydrogen or alternative readily convertible fuels through a controlled electrochemical process [2]. Polymer electrolyte membrane fuel cells (PEMFCs) represent a particularly important class of fuel cells distinguished by their remarkable efficiency and environmentally benign features, fast start-stop and low operation temperature, which are relevant in small or medium-sized portable or mobile applications [3]. It is generally accepted that the major obstacle of the widespread utilization of polymer electrolyte membrane fuel cells is the lack of stable and affordable electrocatalysts [4,5]. Indeed, state-of-art PEMFCs are still constructed with platinum electrocatalysts on high surface area carbon supports. Previous works have clarified the behavior of the Pt/C catalysts at both the anode (in the hydrogen oxidation reaction, HOR) and cathode (in the oxygen reduction reaction, ORR), recognized their limited activity in ORR and identified their degradation pathways such as poisoning with trace amounts of CO from the hydrogen feed, dissolution-redeposition-Ostwald ripening of Pt or electrocorrosion of the carbonaceous support [6–8]. Nevertheless, in spite of many years of intense research [5,8], the commercially viable solution for the electrocatalyst question of the

* Corresponding author.
*E-mail address:* tompos.andras@ttk.hu (A. Tompos).

https://doi.org/10.1016/j.materresbull.2024.113114
Received 14 April 2024; Received in revised form 27 August 2024; Accepted 27 September 2024
Available online 1 October 2024

PEMFC industry is still to use catalysts with extremely high Pt loading, which keeps the price of the cells high and raises sustainability concerns.

It has to be noted that using bimetallic catalysts consisting of alloys of Pt with an oxophilic metal turned out to be a good strategy for enhancing the activity of the Pt/C system in ORR. The alloying elements can involve transition metals [9,10] or post-transition metals like Zn [11] or Sn [12–15] often in the form of ordered $Pt_3M$-type alloys [16, 17]. The beneficial effect of the alloying element is attributed to modifying the electronic structure of the catalyst nanoparticle, resulting in less poisoning by oxygenated spectator species like $OH^-$ [18]. However, dissolution of the alloying element in the acidic milieu of the electrode [18] or even spontaneous rearrangement of the surface structure [19] still leads to stability problems with these types of electrocatalysts.

As an oxophilic transition metal, Mo also seems to be a useful cocatalyst in a Mo-Pt bimetallic system. However, the low miscibility of Mo in Pt, along with the large negative redox potential of the $Mo^{n+}$/metallic Mo couple, render the synthesis of supported Mo-Pt alloy nanoparticles quite difficult [20]. In spite of this, available reports indicate that bimetallic Mo-Pt catalysts indeed are active in ORR [21, 22], in addition to their excellent electrooxidation capability of CO at low potentials [16,23–25]. Nevertheless, apart from the synthesis problems, these kind of alloy electrocatalysts suffer from severe Mo leaching under the working conditions of PEMFCs [26].

Since the stability issues of the Pt/C catalysts are at least partly due to the weak interaction between the platinum nanoparticles and the carbon support, replacement of the latter with an appropriate oxide providing stronger metal-support bonds is a natural idea. Indeed, Pt catalysts on $TiO_2$ [27,28], $SnO_2$ [29,30], $MoO_3$ [31,32] or $WO_3$ [33–35] supports were proposed for PEMFC applications; in these systems the nanoparticle-stabilizing ability of the support may be completed by a synergic co-catalytic effect arising around the metal-oxide junction, resulting, e.g. in enhanced CO tolerance. However, these oxides are often difficult to prepare with suitably high specific surface area and their electrical conductivity is generally too low for electrocatalytic purposes. Moreover, dissolution of the non-noble metal cations from the oxides in acidic medium is quite probable.

An emerging approach focusing mostly on enhancing the multifunctionality of the support, together with increasing its conductivity, is the utilization of mixed oxides, which is typically realized by introduction of a doping element into the $TiO_2$ matrix. Tungsten [36,37], niobium [38–43], molybdenum [44–46] and tin [47,48] are among the frequently studied dopants. In these systems the effect of the dopants on the catalyst activity can be utilized without concerns related to their dissolution, as they remain protected from the aggressive milieu by the titania matrix.

A common feature of the listed oxides is that Pt nanoparticles deposited on them exhibit a range of metal-support interaction phenomena. These may influence the geometrical and/or the electronic structure of the metal particles, involving charge transfer between the metal and the support, but, under specific circumstances, transport of cations from the support to the metal can also occur. Traditionally, this last effect is denoted as strong metal-support interaction (SMSI) [49,50]. Formation of interfacial active sites combining properties arising from both the support and the metallic particle is also a frequent observation [49]. A brief overview of the different manifestations of metal-support interaction is given below in Section 1.2.

Although the stabilization effect of metal-support interactions on the Pt particles is documented in electrocatalytic processes [51–55], and activity enhancement of the oxide-supported Pt particles in the ORR is frequently connected to electronic structure changes associated with electron transfer from the oxide towards Pt [44,46,56], systematic investigations of the metal-support interactions, in particular, their material transport aspects induced by specific pretreatments, was generally out of the scope of these studies.

As it was described above, neither alloy catalysts nor undoped or doped oxide-supported systems offer a complete solution for the requirements of PEMFC electrocatalysts. In an emerging approach, the need for high surface area and electrical conductivity, good corrosion resistance and high extent of stabilization of Pt is realized by an oxide-carbon composite support. The most frequent choice for the oxide component of the composite is $TiO_2$, which is indeed very stable under both reducing and oxidizing conditions in acidic medium, while offers anchoring sites for Pt nanoparticles [56–61], although other oxides were also tested [62].

$TiO_2$ modified with dopants was also proposed for preparation of multifunctional mixed oxide – carbon composite supports with the general formula $Ti_{(1-x)}M_xO_2$-C (M stands for the doping metal). Although the literature on this subject is not as extensive as in the case of carbon-free mixed oxide supports, several examples can still be given, for example $Ti_{(1-x)}Sn_xO_2$–C (x: 0.1–0.3) [63], $Nb_{0.07}Ti_{0.93}O_2$–C [64] and $Ti_{0.9}Ir_{0.1}O_2$–C [65] hybrid support materials were investigated. In our previous efforts W, Mo and Sn were identified as promising dopants for development of novel mixed oxide – carbon composite supports of Pt electrocatalysts in PEMFC applications [66–71]. In these studies, fine tuning of the synthesis of the support for W, Mo or Sn dopants, different oxide/carbon ratios or carbon materials were described. Physicochemical investigations completed with laboratory electrochemistry measurements [66–71] and studies in fuel cell test equipment [72,73] indeed confirmed the performance and the longevity of these electrocatalysts, especially in the HOR at the anode of PEMFCs. It was established that the rutile polymorph of $TiO_2$ is preferred for complete incorporation of the dopant into the titania matrix, which is the prerequisite for long-term stability. At the same time, the atomic closeness of the incorporated dopants and Pt along the perimeter of the metal particles resulted in formation of active sites responsible for the good electrocatalytic performance e.g. in CO oxidation at low potentials [74].

The focus of the mentioned studies was on the structural properties and electrochemical performance of the *as-prepared* mixed oxide – carbon composite supported catalysts. Since Pt and the oxide component of the composite represent a couple in which development of a range of metal-support interactions, involving SMSI is expected, it was plausible to assume that the properties of the Pt/$Ti_{(1-x)}M_xO_2$-C system can be further enhanced by pretreatments inducing transport of species from the oxide towards Pt. Nevertheless, while significant transfer of Sn towards the Pt particles was observed in a Pt/$Ti_{0.8}Sn_{0.2}O_2$-C system hydrogenated at only 200 °C, resulting in massive Sn-Pt alloying, the beneficial effect of the pretreatment on the stability of the catalyst was relatively limited [70]. On the contrary, in case of the Pt/$Ti_{0.8}Mo_{0.2}O_2$-C catalysts, a short preliminary study indicating better long-term behavior after reduction at 250 °C [75] confirmed that it is worth performing a detailed study of the effect of the reductive pretreatment on the structure and performance of the Mo-containing composite supported electrocatalysts.

Nanostructure/nanoparticle preparation methods, involving those used for synthesis of multicomponent materials, result very often in systems in metastable state. Structural changes under elevated temperatures or reaction conditions, which are manifested as instability of the *as-prepared* system, can be regarded as relaxation steps towards a more equilibrium situation. Considering that development of SMSI is actually a similar relaxation process towards a lower energy state, the hypothesis behind the present study is that Pt particles decorated by support oxide-related species due to SMSI must be inherently more stable than either the clean, as deposited particles or those obtained from synthesis routes resulting in bimetallic particles.

The present work focuses on exploring the possibilities offered by SMSI for modulating the properties of Pt/$Ti_{0.8}Mo_{0.2}O_2$-C catalysts. To our knowledge, apart from our short report [75], such investigations were not conducted on similar Mo-containing mixed oxide – carbon composite supported systems. First, a Pt/$Ti_{0.8}Mo_{0.2}O_2$-C catalyst with solid electrocatalytic performance and good long-term stability was selected; it was established in our previous works [69] that a system prepared using $HNO_3$-glucose-functionalized carbon with mixed

oxide/carbon mass ratio of 50/50 is a perfect candidate for this study offering optimal balance between oxide-Pt interactions and longevity. A series of reduced catalysts were prepared by annealing this *as-prepared* material at various temperatures in the 150–450 °C temperature range in hydrogen. Then the structural and surface chemical properties of the *as-prepared* and the reduced catalysts were related to their electrocatalytic performance (activity in the HOR, ORR and CO electrooxidation). During these investigations, a semiquantitative photoelectron-spectroscopic tool was tested for confirming material transport from the support towards Pt. Finally, the degradation of the catalysts was evaluated in 500-cycle and 10,000-cycle electrochemical stability tests in comparison with reference Pt/C catalyst, in order to identify the influence of SMSI on their most important properties.

### 1.2. Overview of metal-support interaction effects

One of the best summaries of the physics behind metal-support interactions can be found in [50].

The growth mode of the metal on the support, determining also the shape of the supported particles, is governed by the relationships between the surface free energies of the metal and the support, along with their interfacial free energy. A modulating factor of the particle geometry is that the crystalline structure of the metal nanoparticle can align to the lattice of the support, resulting in particles with strained lattices, as observed for Pt/$SnO_2$ in ref. [76].

A ubiquitous interfacial process driven by the alignment of the electronic band structure of the metal and the support is the interfacial charge transfer. This can be a short-range effect, e.g. associated with interfacial bond formation, but in case of metal particles on semiconducting oxides, long-range charge transfer, resulting in Schottky barrier formation is frequently observed. Key descriptors predicting the nature of the charge transfer are the reactivity of the metal towards the components of the support (e.g. heat of oxidation of the metal in case of oxides) and difference in the work function between the metal and the support [49,50]. A classic example for the long-range electron transfer is the Pt/$TiO_2$ junction: in this system electrons from the n-type semiconducting $TiO_2$ migrate to Pt, resulting in an electron-rich, negatively charged metal particle, surrounded by an oxide region with positive space charge [50]. The interfacial charge transfer occurring at different length scales can, therefore, contribute to enhancing the bonding of the metal particle to the support, along with modification of its electronic structure.

Another geometric manifestation of metal-support interactions is the transport of support-originated cations to the surface of the metal particles. The ultimate case of this SMSI phenomenon is the complete encapsulation of the metal particle by the (partially reduced) support material as first observed for the Pt/$TiO_2$ couple [50]. While the driving force for this effect is reduction of the total surface free energy of the system, formation of mobile cations seems to be facilitated by presence of defects in the support material and their transport is accelerated by the strong electric field generated by long range electron transfer. Accordingly, this SMSI effect can most easily be induced by reductive pretreatment of high work function, oxidation resistant metal particles deposited onto reducible oxides like $TiO_2$, $SnO_2$ [77], $CeO_2$ [78], etc. Depending on the mutual properties of the metal and the support, decoration of the metal particles by the support material may be accompanied by further reactions such as alloying, as observed in the Pt/$SnO_2$ [77] system.

An important feature of supported catalysts is that specific synergistic reaction sites may develop along the perimeter of the metal-support interface, where, for example, a reactive species activated on the metal particle can react with another species formed on the support [49]. This bifunctional effect explains the CO oxidation activity of Pt at low potentials when in contact with a range of metal oxides [27–35].

Importantly, recent investigations revealed that SMSI-like phenomena are not restricted to Pt-group metals deposited onto reducible oxides and they can be initiated by more gentle treatments than the high-temperature reduction of the classical scenario. For example, it was pointed out that replacing the hydrogen atmosphere by a $CO_2$-$H_2$ gas mixture resulted in a substantial decrease of the encapsulation temperature in Rh/$TiO_2$ or Rh/$Nb_2O_5$ systems through adsorbate-mediated activation of the oxide [79]. SMSI-like material transport was reported under oxidative conditions in metal-oxide couples not sensitive for SMSI in the classical sense (Au/ZnO [80]). The discovery of the concept of reaction-induced SMSI, where encapsulation accompanies surface oxidation or reoxidation of an originally non-oxidic or at least non-reducible oxide support Au/Mo-carbide [81], Ni/BN [82], Au/MgO [83], allowed the design of SMSI-stabilized catalysts on redox-inert supports. The progress in the field, therefore, effectively broadens the choice of the metal/support couples in which the functionality can be tuned by SMSI [51].

## 2. Experimental

### 2.1. Catalyst synthesis

In a previous study Pt/$Ti_{0.8}Mo_{0.2}O_2$-C type electrocatalysts were compared on different carbonaceous supports (native and functionalized Black Pearls 2000, Vulcan XC-72), with varying oxide/carbon ratios [69]. The results indicated that both the use of functionalized carbon and decreasing the amount of oxide resulted in better homogeneity and higher durability of the catalyst [69]. Using this knowledge, a catalyst with 50/50 oxide/carbon weight ratio prepared on $HNO_3$-glucose--functionalized carbon was selected for the purposes of the present work.

Functionalization of the Black Pearls 2000 carbon previously pretreated in nitrogen at 1000 °C with $HNO_3$ and glucose, along with characterization of the resulting material, was described in [68]. Functionalized carbon with 22 % of the surface oxygen-containing functional groups was used in this study. According to previous investigations, these functionalities involved both carboxylic, lactone, phenol or ether-like species from the nitric acid treatment and hydroxyl groups from the glucose treatment [68]. Flow chart and the details of the $Ti_{0.8}Mo_{0.2}O_2$-C composite synthesis and Pt loading of the composite support via a modified, $NaBH_4$-assisted ethylene-glycol reduction-precipitation method can be found in [69]. The starting material of the present study, the freshly synthesized Pt/$Ti_{0.8}Mo_{0.2}O_2$-C catalyst on the composite support containing 50 wt.% of $Ti_{0.8}Mo_{0.2}O_2$ and 50 wt.% $HNO_3$-glucose-functionalized Black Pearls 2000 carbon, loaded with 20 wt.% Pt, is denoted as the *as-prepared* Pt/TiMoC throughout the paper.

Following the synthesis of the *as-prepared* catalyst, fractions of the material were reduced in hydrogen flow under atmospheric pressure in a quartz reactor at temperatures 150 °C, 250 °C, 350 °C and 450 °C for 2 hours, to induce the SMSI effect. These hydrogen treated electrocatalysts are identified by a suffix corresponding to the temperature of the reduction. For example, the catalyst pretreated at 150 °C in hydrogen flow is denoted as Pt/TiMoC-150H, etc.

### 2.2. Structural characterization

Specific surface area of the composite support, the *as-prepared* catalyst and selected reduced catalysts were determined from nitrogen adsorption measurements in a Thermo Scientific Surfer automatic volumetric adsorption analyzer. Structure of the synthesized materials involving both the *as-prepared* and reduced catalysts was investigated by X-ray diffraction (XRD) analysis using a Philips model X'PERT MPD and PW 3710-based PW 1050 Bragg–Brentano parafocusing goniometer, utilizing CuKα radiation, a graphite monochromator, and a proportional counter. The microstructure of the catalysts was characterized by Transmission Electron Microscopy (TEM); the studies were performed by a $C_s$-corrected FEI Titan Themis microscope operating at 200 kV yielding a HRTEM resolution of 0.09 nm. Pt particle size distribution histograms were determined by measuring the diameters of at least 600

randomly selected metal particles from five micrographs of each sample, all collected from non-aggregated regions. Spatial distribution of the components was explored by using the Scanning Transmission Electron Microscopy (STEM) capabilities of the microscope, in connection with energy-dispersive X-ray spectroscopy (EDS) detection. High-resolution micrographs were evaluated and processed using the ImageJ software [84].

### 2.3. Surface chemistry studies

Surface characterizations were conducted using X-ray photoelectron spectroscopy (XPS) with an Omicron EA 125 electron spectrometer. The instrument was operated in the constant analyser energy mode with a pass energy of 30 eV, providing a resolution of approximately 1 eV. Photoelectrons were excited by MgKα radiation. To assess the impact of the reductive treatment, the investigation of the catalysts in their initial, air-exposed state was completed by *in situ* hydrogen exposure steps in the high-pressure/high-temperature treatment chamber of the spectrometer. These *in situ* hydrogen treatment steps were performed for 1 h in 300 mbar $H_2$ at room temperature and 100 °C. Data collected after each treatment phase were processed using the Casa XPS software [85], which involved fitting the data with a combination of Gaussian–Lorentzian peaks, after removal of a linear or Shirley background. Binding energies were referenced to the main C 1s peak of graphitic carbon at 284.4 eV. Quantitative analysis was performed with the XPS MultiQuant software [86,87], assuming a homogeneous distribution of components as described in prior studies [74].

Although the spectral modeling strategy for determination of Mo chemical states was presented in detail previously [74], a short description is still appropriate here. In the fitting procedure of the Mo 3d spectra, the completely oxidized $Mo^{6+}$ ionic state was represented by a simple spin-orbit doublet with its $3d_{5/2}$ component around 232.5 eV; the $3d_{5/2}/3d_{3/2}$ intensity ratio (1:0.66) and doublet separation (3.1 eV) were based on reference spectra of a $MoO_3$ sample. The $Mo^{4+}$ contribution was modeled by a complex line shape arising from coexistence of differently screened final states, with the leading peak around 230 eV; the line shape was derived from measurements on $MoO_2$. $Mo^{5+}$ and more reduced states with the exception of $Mo^{4+}$ were described by spin-orbit doublets with the same line shape (peak separation, intensity- and full-width-at-half-maximum-ratios) as in the case of $Mo^{6+}$, but with lower binding energies (with a $3d_{5/2}$ binding energy around 231 eV for $Mo^{5+}$ and with even lower values of more reduced states if needed). The binding energy ranges of these ionic states were selected consistently with our previous work on the Pt/$Ti_{(1-x)}Mo_xO_2$–C systems [72,74,88] and the relevant literature [89–91].

As it was discussed in ref. [70], because of inelastic mean free path reasons, conventional quantitative XPS measurements are rarely sensitive to decoration of Pt nanoparticles by an ultrathin overlayer. However, the intensity ratio of a low kinetic energy (i.e. low inelastic mean free path, very surface-sensitive) and a high kinetic energy (i.e. higher inelastic mean free path, more bulk-sensitive) Pt feature can serve as an indicator of the buried or exposed state of the surface Pt species. In ref. [70] it was pointed out that the intensity ratio of the Pt NOO Auger peak (64 eV kinetic energy) and the Pt 4f photoelectron peak (1180 eV kinetic energy for MgKα excitation) indeed followed the encapsulation of Pt by Sn-oxide after reductive pretreatment of a Pt/$Ti_{0.8}Sno_{0.2}O_2$-C catalyst. Accordingly, the intensities of these peaks were recorded using the same settings of the electron spectrometer (fixed retard ratio set to 7) during the *in situ* hydrogen exposure experiments performed on the *as-prepared* and reduced Pt/TiMoC electrocatalysts.

### 2.4. Electrochemical characterization

The electrochemical measurements were carried out in a standard three-electrode electrochemical glass cell using a Biologic SP150 potentiostat and the EC-LAB software package. The applied electrolyte was 0.5 M $H_2SO_4$. The catalyst ink was prepared using a Nafion solution (DuPont™ Nafion® PFSA Polymer Dispersions DE 520), isopropanol (Molar Chemicals) and ultrapure water (18 MΩ cm, produced by Millipore equipment). Glassy carbon electrode (d= 0.3 cm, geometric surface A= 0.0707 $cm^2$) was used as working electrode, Pt wire was used as counter electrode and reversible hydrogen electrode (RHE) as reference electrode. All potentials are given on RHE scale.

*As-prepared* and reduced samples were measured by means of cyclic voltammetry (CV) and $CO_{ad}$ stripping voltammetry completed by short (500 CV cycles) and long-term (10,000 CV cycles) stability assessment. The details of the catalyst ink composition and electrocatalytic measurements were described in our previous work [69]; the Pt loading of the electrodes was 10 μg $cm^{-2}$.

In order to evaluate the activity of the samples in the HOR and ORR, steady-state polarization measurements were carried out in the $H_2$ or $O_2$ saturated 0.5 M $H_2SO_4$ solution using rotating disk electrode (RDE) with the same diameter as during CV measurements. The ORR measurements were done at six different rotation speed (225, 400, 625, 900, 1225, 1600 rpm) by sweeping the potential between 1.0 and 0.3 V with 10 mV $s^{-1}$ sweep rate. HOR polarization curves were recorded by sweeping the potential between 0.0 and 0.3 V at 400, 625, 900, 1225 and 1600 rpm rotation speeds, using a sweep rate of 10 mV $s^{-1}$ [92,93].

For comparison, a commercial reference Pt/C electrocatalyst (Quintech C-20-Pt, on Vulcan) with 20 wt.% Pt loading was also studied by the same methods described above.

The electrochemically active surface area (ECSA) of Pt was determined from the charge required to oxidize the monolayer of underpotentially deposited hydrogen [94] using conventional baseline correction as described in ref. [69]. The measure of the ECSA loss after N (N: 500 and 10,000) cycles of the stability test is the ΔECSA value defined in Eq. 1 [69]:

$$\Delta ECSA_N = \{1 - (ECSA_N/ECSA_1)\} \times 100\% \quad (1)$$

where $ECSA_N$ and $ECSA_1$ are the values of the electrochemically active Pt surface area measured in the $N^{th}$ and the first cycle on the same sample, respectively.

## 3. Results

### 3.1. Microstructure of the electrocatalysts

The $N_2$ adsorption isotherms of the TiMoC composite, the *as-prepared* Pt/TiMoC electrocatalyst and the catalysts reduced at 150 °C and 450 °C (Figure S1 in the Supplementary Materials) were qualitatively similar, reflecting the nature of the composite support. The shapes of the isotherms were characteristic for the mixture of a mesoporous carbon and a mesoporous metal oxide component. Specific surface area values were around 400 $m^2/g$ and only minor changes occurred both upon Pt deposition and reductive pretreatments. A concise discussion of the adsorption isotherms and pore size data can be found in the Supplementary Materials (Figure S1 and Table S1).

Structural characteristics of the *as-prepared* Pt/TiMoC electrocatalyst and its reduced counterparts were compared by XRD and TEM, while the surface chemical features were explored by XPS. The X-ray diffractograms are shown in Fig. 1, the electron micrographs are summarized in Figs. 2-3 and in Figures S2-S4 of the Supplementary Materials, while the most important quantitative observations are summarized in Table 1.

Certain physicochemical characteristics of the TiMoC support and the *as-prepared* Pt/TiMoC catalyst were described in [69]. Composition data collected in Table 1 were consistent with those reported in [69] for the *as-prepared* Pt/TiMoC. While the nominal mixed oxide/carbon weight ratio of the composite support was 50/50, the higher apparent C content measured by XPS was repeatedly observed for these systems and the deviation was related to the occurrence of large mixed oxide agglomerates [69,74]. At the same time, composition data determined by

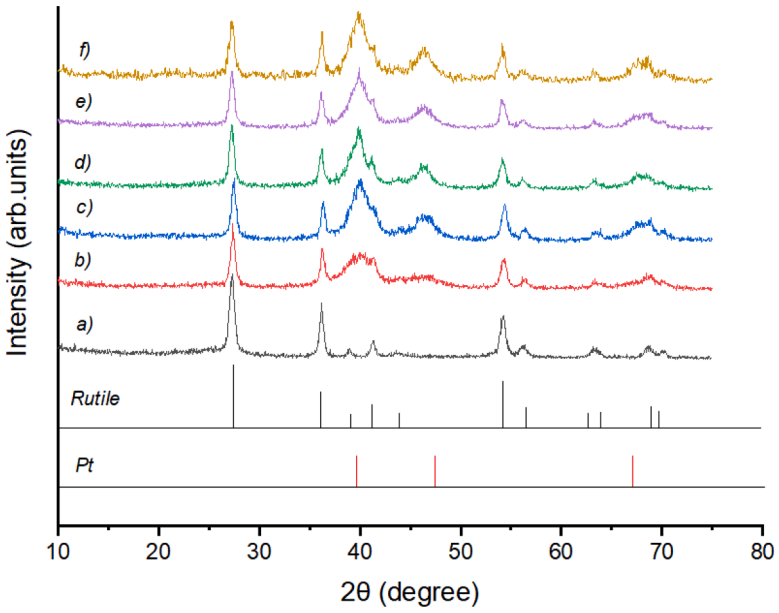


**Fig. 1.** X-ray diffraction patterns of the (a): non-platinized TiMoC composite, (b): *as-prepared* Pt/TiMoC electrocatalyst and its reduced counterparts obtained after treatment at (c): 150 °C, (d): 250 °C, (e): 350 °C and (f): 450 °C in hydrogen flow. Reflection positions for rutile $TiO_2$ and Pt are shown in the bar graphs.

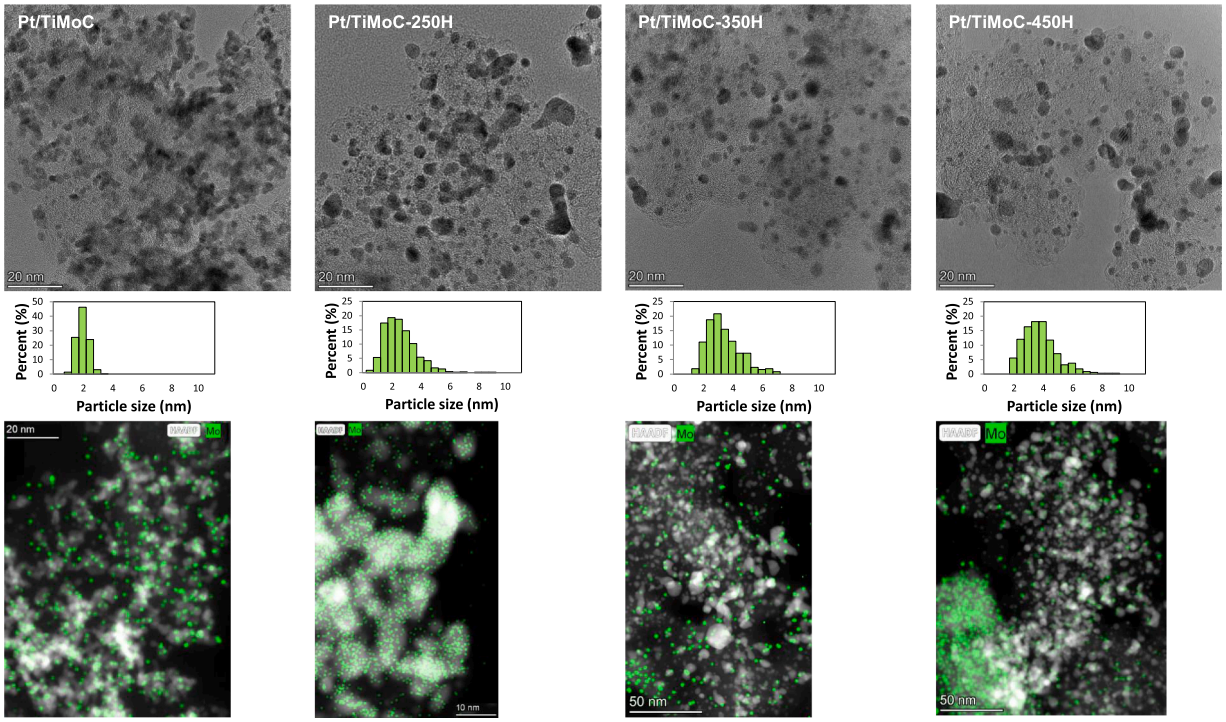


**Fig. 2.** Bright field TEM micrographs (at the top), size distributions (in the middle), HAADF micrographs and Mo elemental maps of the *as-prepared* and reduced Pt/TiMoC electrocatalysts (at the bottom).

STEM/EDS varied around the nominal 50/50 value, although their scatter was considerable due to the very local nature of the method. The Pt content determined by bulk-sensitive techniques such as ICP or EDS was close to the nominal 20 wt.%; the much higher value measured by XPS indicated the surface location of Pt. The Mo/Ti atomic ratio derived from XPS was close to both the nominal value and to the data obtained from bulk-sensitive measurements, suggesting homogeneous molybdenum incorporation into the rutile-$TiO_2$ phase. Importantly, reductive pretreatment caused no significant change in the mixed oxide/carbon mass ratio or the Mo/Ti atomic ratio. The slight decrease of the apparent Pt content measured by XPS after reduction at elevated temperatures suggested some growth of the Pt particles, as confirmed by TEM investigations.

In Fig. 1 XRD patterns of the TiMoC composite (measured before Pt loading) and the Pt-loaded *as-prepared* Pt/TiMoC electrocatalyst are compared with those of the reduced samples. For orientation, the reflections expected from metallic Pt (JCPDS 04-0802) and rutile $TiO_2$ (JCPDS 21-1276) are shown as bar graphs. As it was mentioned in our previous works [68,72], the synthesis of this composite resulted in exclusive formation of the rutile-$TiO_2$ phase; no separated crystalline

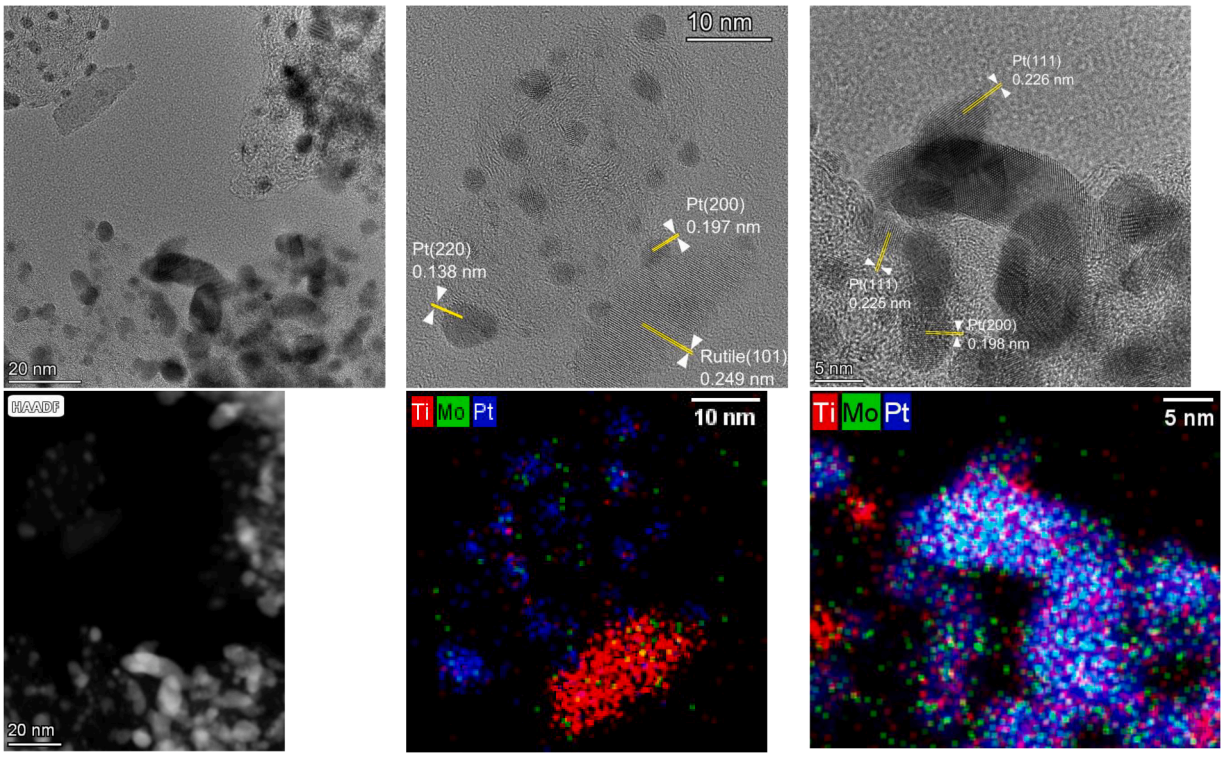


**Fig. 3.** TEM images of the Pt/TiMoC-250H electrocatalyst (at the top) and HAADF image and elemental maps of Pt, Ti and Mo obtained in the selected fragments (at the bottom). Color code: Pt (blue), Ti (red), Mo (green).

**Table 1**
Composition and structural characteristics of the *as-prepared* and reduced Pt/TiMoC electrocatalysts.

| Sample/ Treatment | Catalyst composition (wt.%) | | | | Atomic ratios | | Pt particle size (nm) | |
|---|---|---|---|---|---|---|---|---|
| | XPS | | STEM/EDS | | XPS | STEM/EDS | | |
| | Oxide/C[a] | Pt | Oxide/C | Pt | Mo:Ti | Mo:Ti | XRD | TEM |
| **Pt/TiMoC** | 33/67[b] | 39[b] | n.a. | 18[b,c] | 1:4.3[b] | 1:5.7[b,c] | 2–3 | 2–3 |
| **Pt/TiMoC–150H** | 30/70 | 35 | n.a. | n.a. | 1:4.5 | n.a. | 3–4 | n.a. |
| **Pt/TiMoC–250H** | 31/69 | 39 | 53/47 | 25 | 1:4.3 | 1:4.9 | 3–4 | 2–3.5 |
| **Pt/TiMoC–350H** | 28/72 | 34 | 35/65 | 15 | 1:4.1 | 1:4.7 | 3–4 | 3–4 |
| **Pt/TiMoC–450H** | 29/71 | 33 | 44/56 | 17 | 1:4.3 | 1:4.8 | 3–4 | 3.5–4.5 |

[a] Calculated without the Pt content
[b] From ref. [69]
[c] Measured by ICP

anatase $TiO_2$ or Mo-oxide phases were detected. Nevertheless, a shift of the rutile reflections with respect to those of pure $TiO_2$ indicated distortion of the unit cell as a result of Mo incorporation [69,95]. The amount of Mo built into the rutile lattice (~18%) was very close to the nominal Mo content, giving another indication of the almost complete Mo incorporation. Pt loading caused no changes in the structure of the mixed oxide; however, broad reflections from nanosized Pt particles appeared. Estimation of the Pt particle size with the Scherrer equation suggested the formation of 2–3 nm crystallites in the *as-prepared* Pt/TiMoC. This fine particle size is the characteristic feature of the applied modified $NaBH_4$-assisted ethylene glycol reduction–precipitation technique [67]. Reductive pretreatment resulted in a slight narrowing of the Pt reflections, indicating some growth of the metal particles to 3–4 nm during the 150 °C treatment step. Essentially no changes were observed after $H_2$ treatments at higher temperatures, demonstrating the particle stabilizing capability of the composite support. Reflections arising from the oxide phase of the composite remained unchanged during the reductive pretreatments.

In Fig. 2 transmission electron micrographs of the *as-prepared* Pt/TiMoC catalysts and its counterparts reduced at 250 °C, 350 °C and 450 °C are shown. High resolution micrographs and elemental maps of Pt/TiMoC-250H are presented in Fig. 3, while similar images for the other studied catalysts are given in Figures S2-S4 in the Supplementary Materials. In principle, micrographs of both the *as-prepared* and the reduced catalysts revealed relatively homogeneously dispersed dark nanoparticles over the support. According to either EDS elemental maps recorded in the STEM mode of the microscope or to d-spacing values measured on high resolution micrographs (see Fig. 3 and Figures S2-S4), these nanosized features were identified as Pt particles. The contrast of the oxide component was quite similar to that of the carbonaceous backbone; nevertheless, elemental maps at lower magnification showed congruent distribution for Pt, Ti and Mo (e.g. Figure S2, *as-prepared* Pt/TiMoC electrocatalyst), while smaller Ti-rich oxide particles among the Pt particles were revealed at higher magnification (e.g. Fig. 3, Pt/TiMoC-250H or Figure S3, Pt/TiMoC-350H). Similarly, high resolution micrographs confirmed the coexistence of Pt particles and rutile features over the carbonaceous backbone (Fig. 3 and Figures S2-S4) in both the *as-prepared* and the reduced catalysts.

A key feature responsible for the electrocatalytic behavior of these catalysts is the relationship between the distribution of Mo and Pt.

Occurrence of Mo in the vicinity of Pt was demonstrated by overlapping the HAADF-STEM micrographs of the catalysts with the elemental maps of Mo (at the bottom of Fig. 2). Due to the contrast mechanism of the HAADF imaging, the most strongly scattering Pt particles were the brightest features. Significant Mo enrichment coincided with larger oxide particles (such as at the lower left corner of the image of Pt/TiMoC-450H in Fig. 2), but Mo signals were consistently detected over the Pt-covered regions, regardless to the pretreatment state of the catalyst. It has to be mentioned that noise in the elemental maps was reduced by averaging over several pixels. Although the area of averaging was kept under the characteristic size of the Pt particles, it resulted in a more washed image than the HAADF micrograph. Considering this together with the fact that microscope settings providing slightly different sensitivity and spatial accuracy were used in collecting the maps for the different catalysts, looking for more subtle details in these elemental distributions is impractical.

The relatively homogeneous appearance of the electrocatalysts is in agreement with the conclusions of ref. [69], where it was established that increasing the amount of the carbonaceous fraction of the composite support results in increasing homogeneity of the catalyst.

The Pt particle size distributions of Fig. 2 suggest that the reductive pretreatment resulted in some growth of the catalyst particles. In agreement with the XRD data, the Pt particle size was around 2 nm in the *as-prepared* Pt/TiMoC system. Upon reduction, a fraction of the particles coalesced, providing a broader size distribution with a tail towards the larger particles. While the typical Pt particle size remained in the 2–3 nm range after the 250 °C reduction step, a slight shift towards larger values was observed after reduction at higher temperatures (see also Table 1). Nevertheless, Pt remained finely dispersed even after hydrogen treatment at 450 °C.

At the same time, the elemental maps of Figs. 2-3 and Figures S2-S4 indicate that the reductive pretreatment had very little effect on the distribution of Mo or Ti. In both the *as-prepared* Pt/TiMoC catalyst and its reduced counterparts close coupling between the oxide component and Pt was evidenced, resulting in ample formation of Pt/oxide/carbon triple junctions in all investigated systems.

### 3.2. Surface chemistry of the as-prepared and reduced electrocatalysts

Previous XPS studies established that the response of the Pt-$MoO_x$-containing surfaces, such as the Pt/$Ti_{(1-x)}Mo_xO_2$–C composite supported electrocatalysts or a model system consisting of an ionic Mo monolayer on Pt to hydrogen exposure at room or slightly elevated temperatures is determined by spillover of hydrogen activated on Pt towards the oxide [74]. Hydrogen treatment of the Pt/$Ti_{(1-x)}Mo_xO_2$–C catalysts with indirect Mo-Pt connections at the Pt/oxide junctions resulted in significant reduction of the Mo component to mainly the $Mo^{4+}$ but to a smaller extent to a $Mo^{2+}$-$^{3+}$-like state. In case of Mo ions directly deposited on Pt, however, reduction of Mo to the metallic state was observed, leading to the formation of a Mo-Pt surface alloy which was only partly re-oxidized after subsequent air exposure. This observation allowed to develop a method for spectroscopic identification of Mo species in direct contact with Pt. In ref. [75] we found that the sensitivity of the method was enough to demonstrate transfer of Mo towards Pt during reductive pretreatment at 250 °C. The same approach, consisting of *in situ* hydrogen exposure of the samples in the electron spectrometer, was applied in the present work to probe the changes in the oxide-Pt interaction induced by the reductive pretreatment at various temperatures.

XPS investigation of the *as-prepared* Pt/TiMoC electrocatalyst revealed features consistent with previous results on Pt/$Ti_{(1-x)}Mo_xO_2$–C composite supported systems [72,74,88]. Shortly, the Pt content was almost exclusively metallic with the Pt $4f_{7/2}$ peak at 71.3 eV binding energy; trace amounts of ionic Pt appeared due to storage under atmospheric conditions. The Ti content was completely oxidized as evidenced by the Ti $2p_{3/2}$ peak at 458.7 eV. The C 1s spectrum was adequately modeled by the combination of the asymmetric line shape of graphitic carbon (main peak at 284.4 eV) and small (few percent) contributions of singly (peak at 286–286.4 eV) or more oxidized (peak around 288 eV) carbon atoms. The appearance of these oxygen-bound carbon species was the consequence of the use of functionalized carbon for composite preparation [68]. The Mo 3d spectrum (illustrated in Fig. 4, panel A, uppermost trace) was processed as described in [74]; it was dominated by signals from $Mo^{6+}$ ions (Mo $3d_{5/2}$ binding energy at 232.5 eV), but deconvolution revealed the presence of smaller amounts of $Mo^{5+}$ (231.2 eV) and $Mo^{4+}$ (229.8 eV) states as well.

As it was mentioned above, in order to explore the changes in the surface chemical state of the catalysts induced by the reductive pretreatment, XPS data were collected in both the *as-received* (air exposed) state of the electrocatalysts and after *in situ* $H_2$ exposure in the electron spectrometer. Pt 4f, Mo 3d, Ti 2p and C 1s binding energies recorded during these experiments are collected in Table S2 and the Mo 3d spectra are presented in Fig. 4.

As it can be seen in panel A of Fig. 4, the Mo 3d spectra of all catalysts were very similar in the air exposed state. The dominant contribution arose from the $Mo^{6+}$ ionic states (with a $3d_{5/2}$ binding energy around 232.5 eV); the asymmetry on the low binding energy part of the spectrum indicated the presence of more reduced Mo species and was adequately modeled by $Mo^{5+}$ ($3d_{5/2}$ binding energy slightly above 231.0 eV) and $Mo^{4+}$ (around 230.0 eV) contributions. However, a closer comparison of the low binding energy tails of the Mo 3d spectra of the *as-received* catalysts suggested the presence of a further, very weak component (accounting for only a few percent of the total Mo signal) in the spectra of all reduced catalysts. Curve fitting indicated a $3d_{5/2}$ binding energy around or slightly below 229.0 eV for this new component. This value is too low for $Mo^{4+}$ or even the unstable $Mo^{2+}$-$^{3+}$ observed during annealing of Pt/$Ti_{(1-x)}Mo_xO_2$–C catalysts in hydrogen (around 229.5 eV) but is entirely consistent with metallic Mo alloyed with the Pt surface [74]. The presence and assignment of this new component was confirmed by the *in situ* room temperature hydrogen exposure experiment: although the $Mo^{5+}$-$Mo^{4+}$ contributions increased in all catalysts on the expense of the $Mo^{6+}$ peaks, a particular enhancement of the low binding energy tail region due to increase of the metallic signal was evident only in the reduced samples especially in those pretreated at or above 250 °C. These reductive pretreatment-related new Mo signals coincided with the Mo 3d doublet of the Mo-Pt surface alloys. Therefore, XPS investigations combined with *in situ* hydrogen exposure demonstrated the appearance of new, special Mo species in all reduced catalysts, which were very easily reducible to a metallic, Mo-Pt surface alloy-like state. As these Mo species were missing from the *as-prepared* Pt/TiMoC catalyst, one can conclude that they were transferred to the Pt as the result of the reductive pretreatment, in analogy with the strong metal-support interaction phenomenon. Our observations indicate that a pretreatment temperature of 150 °C is enough for initiating this transport process. Comparison of the spectra of the reduced catalysts after *in situ* hydrogen exposure suggests that there may be a correlation between the pretreatment temperature and the extent of Mo transport to Pt, although the low signal intensity and the overlapping nature of the different Mo contributions hinder the quantification of this effect.

In a supporting experiment, the *as-prepared* Pt/TiMoC catalyst was annealed in hydrogen in the electron spectrometer at temperatures ranging from room temperature to 300 °C. Mo 3d spectra recorded during this series are presented in the Supplementary Materials section as Figure S5. Not surprisingly, the behavior of the Mo 3d peaks was very similar to that described in ref. [74] for a similar electrocatalyst: gradual reduction of Mo occurred, due to spillover of hydrogen activated on Pt towards the oxide. The reduction of Mo was almost completely reversible upon air exposure. In order to follow the exposed/buried state of Pt during this experiment, the variation of the intensity ratio of the low kinetic energy Pt NOO Auger peak and the high kinetic energy Pt 4f peak was also recorded (see also Sect. 2.3 in the Experimental section) and is shown in Fig. 5.

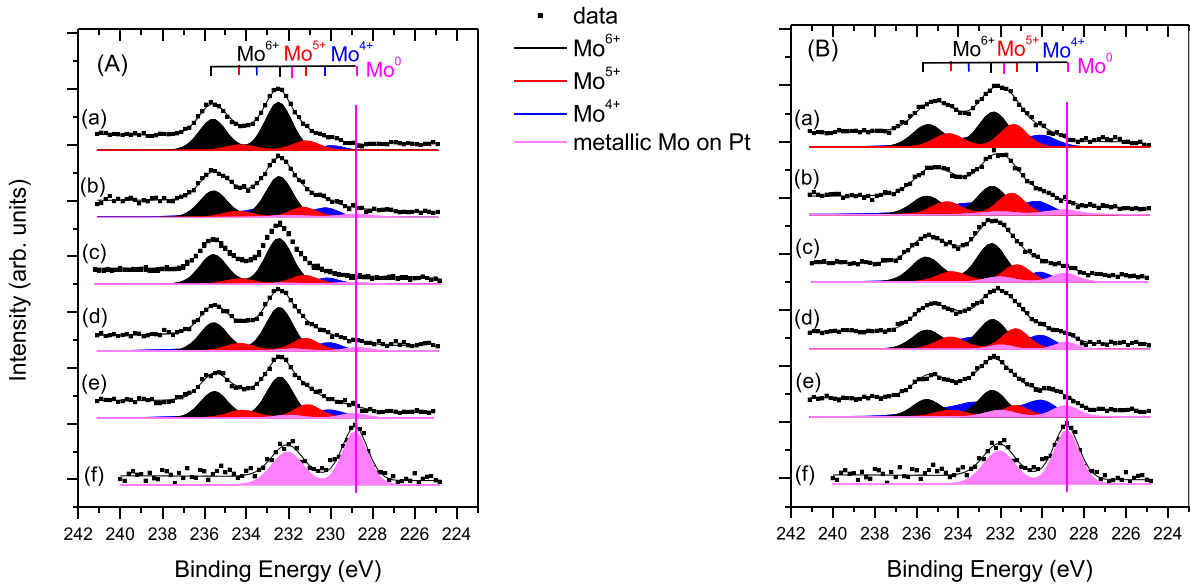


**Fig. 4.** Mo 3d spectra of the *as-prepared* Pt/TiMoC electrocatalyst (a), the reduced electrocatalysts Pt/TiMoC-150H (b), Pt/TiMoC-250H (c), Pt/TiMoC-350H (d), Pt/TiMoC-450H (e), and a Mo-Pt surface alloy containing metallic Mo ((e), from [74]). Panel (A): *as-received* (air exposed) state of the catalysts. Panel (B): *in situ* hydrogen exposed state of the catalysts (300 mbar $H_2$ treatment at room temperature in the preparation chamber of the electron spectrometer for 1 h).

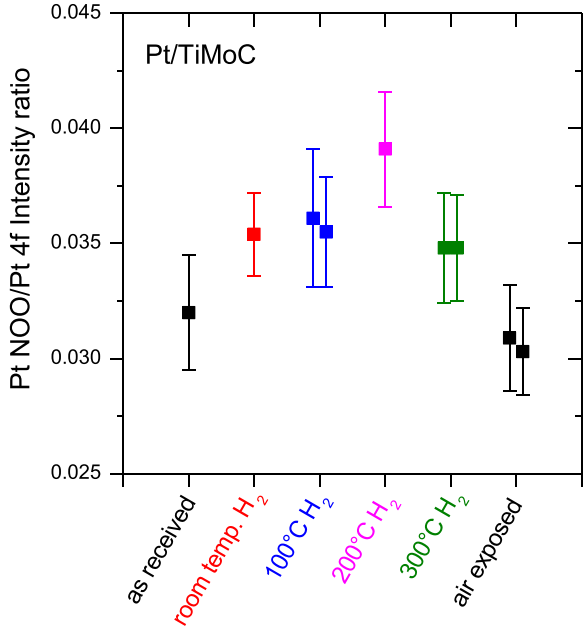


**Fig. 5.** Variation of the Pt NOO (64 eV)/Pt 4f (1180 eV kinetic energy) intensity ratio during *in situ* reduction of the *as-prepared* Pt/TiMoC catalyst in the electron spectrometer completed by air exposure. The hydrogen exposure steps were performed in 300 mbar $H_2$ for 1 h at the temperatures indicated below the graph. The error bars represent scatter of the ratio which was mainly due to uncertainties in the measurement of the Pt NOO intensity. Several measurements were performed in duplicate, indicating the good reproducibility.

The intensity ratio (Fig. 5) revealed an initial increase, a maximum around 200 °C hydrogen treatment temperature and a clear decrease after treatments at higher temperatures. The increase of the ratio at the beginning of the reduction series can be attributed to desorption of surface contaminants, resulting in more exposed Pt surface species. However, the decrease at temperatures higher than 200 °C suggested burial of the Pt surface by foreign species, which as described above, can be identified as Mo species originating from the support. The decrease of the ratio after air exposure can be attributed to oxidation of the partly reduced Mo layer. Adsorption of atmospheric contaminants was less important: outgassing the sample at 100 °C after the air exposure did not change the measured ratio beyond the experimental uncertainties.

Although the conditions of this *in situ* hydrogenation series were different from that of the reductive pretreatment used in catalysts preparation, the results still confirm that material transport towards Pt occurred mainly from 200 °C treatment temperature.

While the reductive pretreatment did not influence the Pt 4f and Ti 2p spectral line shapes, a slight but reproducible variation of the Pt $4f_{7/2}$ and Ti $2p_{3/2}$ binding energies with respect to the C 1s peak of the graphitic carbon component was induced by the *in situ* hydrogen exposure in the electron spectrometer in case of all investigated samples (Table S2). We believe that the small shift of the Pt peaks towards lower and the Ti peaks towards higher binding energies is due to electron transfer from the oxide towards the Pt particles; this effect is presumably the manifestation of the electronic aspect of the metal-support interaction. Our observations suggest that this kind of electronic coupling can be enhanced under reductive conditions. At the same time, it can be observed both in the *as-prepared* and reduced electrocatalysts, so it is not connected to the reductive pretreatment.

### 3.3. *Electrochemical characteristics of the as-prepared and reduced electrocatalysts*

The electrocatalytic properties of the *as-prepared* Pt/TiMoC material and its reduced counterparts treated in hydrogen at 150 °C-450 °C were investigated by electrochemical measurements in a classic three-electrode system as well as by a RDE technique. The study consisted of CV, $CO_{ads}$ stripping voltammetry and stability evaluation through continuous cycling (500 and 10,000 cycles) within the potential limits of 0.05–1.00 V. RDE measurements were used to assess the activity in the ORR and HOR. The results were compared with data obtained on a commercial reference Pt/C catalyst.

Fig. 6 presents a summary of the cyclic voltammograms for both the *as-prepared* and the hydrogen pretreated electrocatalysts. To get information about short-term changes of the catalysts, CVs were recorded before and after short 500-cycle stability tests. The voltammograms primarily revealed features related to platinum. In the 0.05–0.35 V potential range desorption/adsorption peaks attributed to underpotentially deposited hydrogen were observed; these peaks signify the

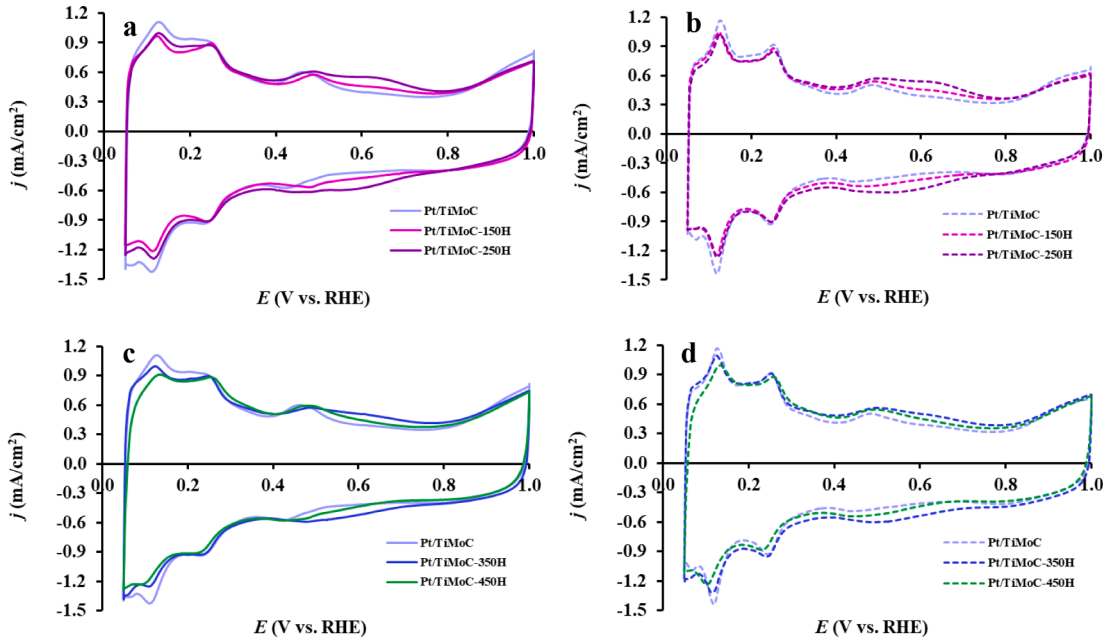


**Fig. 6.** Cyclic voltammograms of the *as-prepared* ( ) and 150 °C ( ), 250 °C ( ), 350 °C ( ) and 450 °C ( ) reduced Pt electrocatalysts obtained before (a, c) and after the 500-cycle stability test (b, d). Recorded in 0.5 M $H_2SO_4$ at 100 mV·$s^{-1}$, T= 25 °C.

reversible adsorption and desorption processes associated with hydrogen at the electrode surface. These signals are related to the accessibility of Pt to hydrogen and were used to estimate the ECSA of the catalysts. Furthermore, the voltammograms depicted oxidation/reduction peaks of Pt above 0.80 V. Importantly, a redox peak pair associated with molybdenum was consistently observed in the potential range of 0.38 to 0.53 V. The presence of these redox peaks in the voltammograms serves as a clear confirmation of an active interface between the platinum nanoparticles and the surface Mo species within the composite support [67–69,88,95,96]. Observations described above were further supported by comparing CVs of the composite support and the *as-prepared* Pt/TiMoC electrocatalyst (Figure S7 in the Supplementary Materials). Marginal changes of the support were revealed during the 500-cycle stability test. At the same time, CVs in Fig. 6a and 6b or 6c and 6d indicate that the Mo oxidation/reduction peak pair became somewhat weaker during the 500-cycle aging in case of the *as-prepared* electrocatalyst, while hardly any change occurred in case of the reduced catalysts.

The electrochemically active Pt surface area of the electrocatalysts measured in the first cycle ($ECSA_1$) is listed in Table 2. While a relatively high ECSA value was obtained for the *as-prepared* Pt/TiMoC catalyst, a small but consistent decrease was observed for all reduced catalysts. It should be noted that for all reduced samples, according to Table 2, quite close $ECSA_1$ values (lying within the range of the experimental errors) were obtained in the range of 55.7±1.9 $m^2/g_{Pt}$, regardless to the reduction temperature.

The ECSA loss (ΔECSA) with respect to the number of stability test cycles was determined from charges associated with hydrogen desorption in the initial and subsequent cycles ($500^{th}$ or $10{,}000^{th}$) (for details see ref. [69] and Experimental part). The ECSA decrease of the reduced catalysts can be explained by either a decrease of the accessibility of the Pt surface by adsorption of impurities and/or partial encapsulation by mobile Mo oxide species or by slight increase of the Pt particle size during the reduction treatments [75]. Although TEM investigations indeed revealed some particle growth (see Fig. 2), the ECSA change observed during the 500-cycle short-term stability test (Fig. 7a) indicated that partial blocking of the catalyst surface after the reduction pretreatment is more important. Namely, as shown in Fig. 7a, an initial

**Table 2**
Electrochemical performance of the reference Pt/C and $Ti_{0.8}Mo_{0.2}O_2$-C composite supported Pt catalysts: the position of the main CO oxidation peak determined from the $CO_{ads}$-stripping analysis, ECSA and its changes during the short- and long-term stability tests and current density measured in the ORR at 0.80 V.

| Sample | $E_{CO,max}$, mV[a] | $ECSA_1$, $m^2/g_{Pt}$ | $\Delta ECSA_{500}$, % [b] | $\Delta ECSA_{10,000}$, % [b] | *j* @ 0.8 V, mA/$cm^2$[c] |
|---|---|---|---|---|---|
| **Pt/TiMoC** | 745 [d] | 68.1 ± 3.0 | 8.1 | 32.2 | 1.09 |
| **Pt/TiMoC-150H** | 745 [d] | 54.2 ± 2.4 | 2.8 | 27.5 | 1.38 |
| **Pt/TiMoC-250H** | 745 [d] | 53.9 ± 2.7 | 3.0 | 23.8 | 1.68 |
| **Pt/TiMoC-350H** | 755 [d] | 57.0 ± 1.9 | -2.9 | 22.1 | 1.51 |
| **Pt/TiMoC-450H** | 755 [d] | 57.7 ± 2.4 | 0.6 | 28.0 | 1.55 |
| **Pt/C** | 795 | 87.2 ± 2.3 | 12.7 | 47.8 | 1.63 |

[a] The position of the main CO stripping peak;
[b] $\Delta ECSA_{500}$ and $\Delta ECSA_{10,000}$ were calculated from the charges originated from the hydrogen desorption in the $1^{st}$ and $500^{th}$ or $10{,}000^{th}$ cycles according to the Eq. 1 (see Experimental part);
[c] Current density at 0.80 V measured in RDE experiments at 900 rpm;
[d] Center of two overlapping CO stripping peaks.

increase of the ECSA of the reduced catalysts was observed in all cases during the first 100–150 cycles (although the 5–10% change was just slightly higher than the range of uncertainties), which can be interpreted as surface cleaning of the catalyst, eliminating impurities or oxides that could potentially impede hydrogen adsorption [92].

After ca. 200 cycles decrease of ECSA was recorded in all reduced catalysts (see Fig. 7a), however, this decline remained moderate, with the relative loss consistently smaller than that of the *as-prepared* sample or the reference Pt/C catalyst, indicating improved stability due to the reductive pretreatment.

In the preparation of composites, the goal of carbon functionalization was to increase the density of functional groups, leading to increased hydrophilicity and improved interaction between the carbon and the growing rutile-$TiO_2$ phase, which has some positive effect on the formation of a uniform layer of very fine mixed oxide NPs over the carbonaceous backbone [68]. Numerous examples in the literature indicate that catalysts of this type have better dispersion of metal nanoparticles, improved electrocatalytic performance and increased

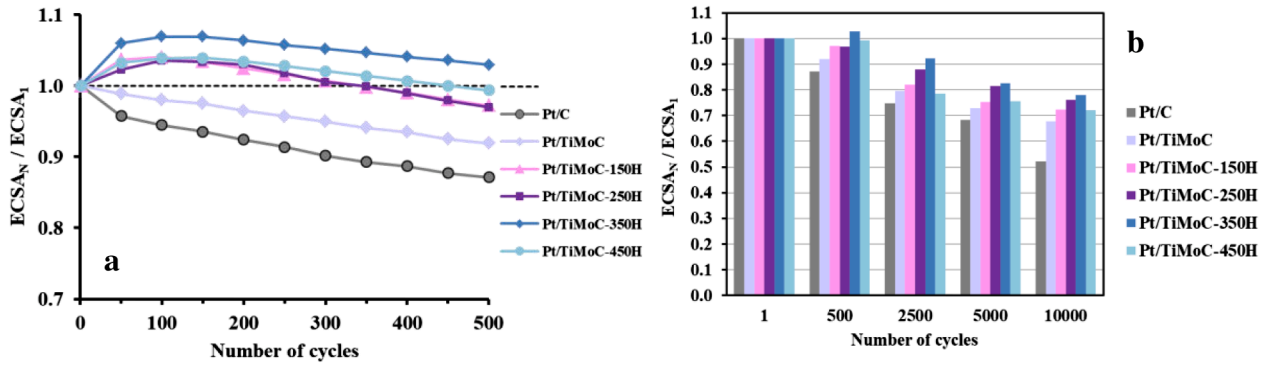


**Fig. 7.** ECSA change during 500 CV cycles (a) and 10,000 CV cycles (b) for the *as-prepared* Pt/TiMoC ( ) and its reduced counterparts: Pt/TiMoC-150H ( ), Pt/TiMoC-250H ( ), Pt/TiMoC-350H ( ) and Pt/TiMoC-450H ( ). Results obtained on the reference Pt/C ( ) were included for comparison. $ECSA_N/ECSA_1$: comparison of the ECSA measured after N cycles normalized to ECSA measured in the 1st cycle of both the *as-prepared* and $H_2$-reduced catalyst as a function of the number of cycles (N).

stability [97–99]. Thus, $Pt/TiO_2/C$ catalysts synthesized using glucose-pretreated Vulcan XC-72 had excellent ORR activity and high durability during accelerated stress tests [100].

Our previous studies revealed that the *as-prepared* Pt/TiMoC catalyst prepared using $HNO_3$-glucose-functionalized carbon with mixed oxide/carbon ratio of 50/50 was among the best ones in the long-term stability tests, significantly surpassing the performance of Pt/C references [69, 75]. This result is reflected in Figure 7b; however, even lower ECSA loss values were recorded for the reduced catalysts. Reductive pretreatments performed at 250 °C or 350 °C had the most beneficial effect on the stability, resulting in ECSA loss of some 20% after 10,000 polarization cycles (see Table 2). A somewhat worse behavior was found for the catalyst reduced at 450 °C. Analogous results in terms of stability were observed in PtNiMo ternary alloy [101]; in that study the introduction of acid-resistant Mo atoms in the alloy stabilized the near-surface Pt atoms, which resulted in significantly higher catalyst stability compared to reference Pt/C.

The changes of the shape of the cyclic voltammograms obtained during the 10,000-cycle stability test for the *as-prepared* Pt/TiMoC and reduced Pt/TiMoC-350H electrocatalysts are demonstrated in Figure 8; the corresponding cyclic voltammograms obtained on other reduced catalysts are presented in Figure S6 in the Supplementary Materials. As shown in Fig. 8b, on the reduced catalyst, the slight changes in the voltammograms are mainly related to features associated with hydrogen desorption/adsorption in the 0.05–0.35 V potential range and Pt oxidation/reduction peaks above 0.80 V. The difference between *as-prepared* and reduced catalysts is mainly related to the double-layer region (*cf.* cyclic voltammograms in Figs. 8a and 8b): for the reduced Pt/TiMoC-350H catalyst, the double-layer region remains almost unchanged, indicating an increase in the stability of the system after reductive pretreatment. While, as shown in Fig. 8a, the Mo oxidation/reduction peaks of the *as-prepared* Pt/TiMoC catalyst undergo more significant changes.

Efficient CO electrooxidation is crucial for maintaining the performance and durability of fuel cell systems [4], as the presence of CO can poison catalysts and degrade their activity over time [2]. The ability of molybdenum to adsorb hydroxyl groups ($OH_{ads}$) according to a bifunctional mechanism is responsible for the increased CO tolerance of Mo-containing catalysts at very low electrode potentials [102,103].

$CO_{ads}$ stripping voltammetry studies were performed to assess the activity of the *as-prepared* catalyst and its reduced counterparts in CO oxidation as depicted in Fig. 9. As it was discussed in our previous works, the most important indicator of the low potential CO electrooxidation activity of these catalysts is the enhancement of current in the pre-peak region (0.05–0.50 V), preceding the main CO oxidation peak. The pre-peak region involves contributions from the oxidation of weakly bound CO on Pt by spillover of OH species formed on neighboring Mo sites, as well as from the Mo redox feature [88]. It should be noted that these "pre-peaks" are typical for Ti, Ta, W, and Mo suboxide-containing Pt electrocatalysts [104,105]. Thus, its presence in the $CO_{ads}$ stripping voltammogram demonstrates the close proximity of Pt and easily reducible Mo species [49,68,106,107]. It must be noted that, according to the literature, a decrease or even disappearance of the Mo redox peaks after long-term cyclic polarization is usually accompanied by a decrease of the "pre-peak" intensity and a shift of the main CO electrooxidation peak towards a higher potential [108].

In agreement with our previous works, favorable CO electrooxidation performance was observed for both the *as-prepared* Pt/TiMoC catalyst and its reduced counterparts. However, the pre-peak region of the reduced catalysts was in all cases more pronounced than that of the *as-prepared* system. Even more importantly, while significant decrease of the current density in the pre-peak potential range was observed for the *as-prepared* catalyst after the 500 cycle short-term stability test, practically no change occurred in the reduced materials. The most plausible

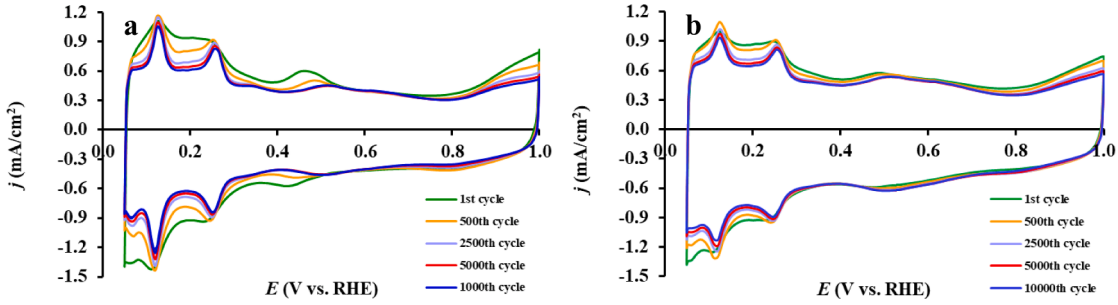


**Fig. 8.** Cyclic voltammograms of the *as-prepared* Pt/TiMoC (a) and Pt/TiMoC-350H (b) electrocatalysts obtained during 10,000-cycle stability test. Recorded in 0.5 M $H_2SO_4$ solution with 100 mV $s^{-1}$ sweep rate, T= 25 °C.

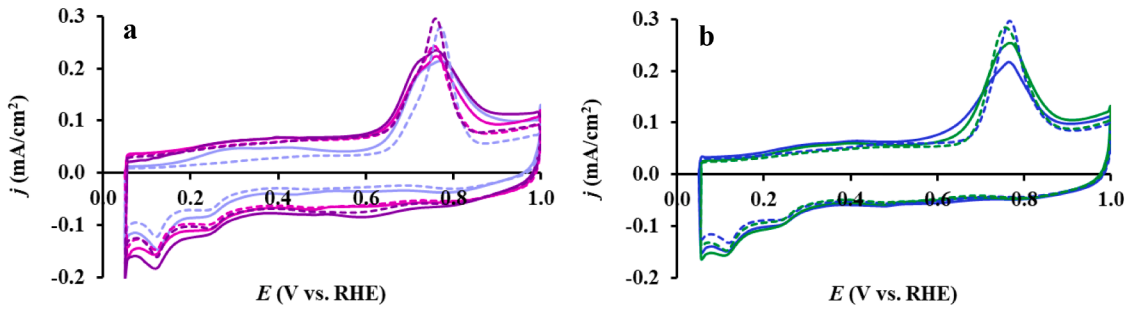


**Fig. 9.** Effect of the reduction temperature on the electrocatalytic performance of the Pt/TiMoC catalysts: (a) *as-prepared* ( ) and reduced at 150 °C ( ) and 250 °C ( ) catalysts, and (b) catalysts reduced at 350 °C ( ) and 450 °C ( ). The $CO_{ads}$ stripping voltammograms were recorded in 0.5 M $H_2SO_4$ before (solid curves) and after 500 cycles (dashed curves) of the stability test. Polarization rate: 10 mV·s$^{-1}$, T= 25 °C.

interpretation of this finding is the enhancement of the Mo-Pt coupling during the reductive pretreatment, which is achieved by transfer of Mo to the surface of the Pt particles, as discussed in the previous section. Importantly, both short- and long-term aging tests (Figs. 7 and 8) indicate the very strongly bound, stable nature of these Mo species formed during the reductive pretreatment process. While in Mo-Pt alloy electrocatalysts leaching of Mo was observed [24], we believe the stability of the Pt-bound Mo species obtained in this study reflects the more equilibrium nature of the catalyst formation via SMSI compared to other synthesis routes like co-reduction [20,24] used for preparation of alloy catalysts.

It should be noted that a relatively broad main peak, corresponding to the oxidation of CO strongly bonded to Pt, was observed on all the samples at about 0.75 V (see Fig. 9 and Table 2) with a good agreement with previous research [75]. Its slight shift towards less positive potentials than in Pt/C is another sign of the enhanced CO electrooxidation capability of the Mo-containing Pt systems, which can be attributed to the electronic aspects of the metal-support interaction.

Although – predominantly because of their good CO electrooxidation capabilities – the Pt/$Ti_{(1-x)}Mo_xO_2$-C composite supported electrocatalysts are mainly recommended for HOR, it may be worth to investigate their properties in the ORR as well. The activity of the *as-prepared* and reduced catalysts was tested in the ORR in a three-electrode system using RDE in 0.5 M $H_2SO_4$ solution saturated with $O_2$. Catalytic activity was investigated after 10 cycles of cleaning at six rotation speeds (for details see Experimental part). The expected current density increase in the potential dynamic polarization curves at higher rotation rates (not shown) was demonstrated for all catalysts, indicating faster diffusion of oxygen to the surface of catalysts.

To compare the investigated catalysts, potential sweeps in the kinetically controlled, mixed kinetic-diffusion controlled and the diffusion-limited regions measured at 900 rpm are depicted in Fig. 10a-b. As can be seen from Fig. 10a-b, very similar values of diffusion-limited current densities were achieved on the reference Pt/C and all reduced catalysts with the exception of the *as-prepared* Pt/TiMoC catalyst. In the presence of an intact, non-porous catalyst layer, the diffusion-limited current density ($j_{lim}$) on the working electrode should theoretically always be the same, since it depends solely on the rotation speed according to the Koutecký–Levich equation. However, according to the literature, the lower $j_{lim}$ can be attributed to reversible oxide formation/reduction on Pt [109] or to the different morphology and/or structural characteristics of the support. However, it should be noted that the deviation of $j_{lim}$ values observed in Fig. 10a was within the range of expected relative measurement errors mentioned by Mayrhofer *et al.* [110] for $j_{lim}$ values observed in the ORR measurements on carbon-containing supported catalysts which was about 10%.

The onset potential of ORR for all the samples was close to that observed on Mo-doped composite supported catalysts and was around 965 ± 10 mV [93], indicating high activity in this reaction. As shown in Fig. 10a-b, in the case of the mixed kinetic-diffusion controlled region, the ORR current density measured on the catalysts reduced at or above 250 °C was very close to or even exceeded that of the reference Pt/C catalyst. However, the current density of the *as-prepared* sample (at 0.8 V vs. RHE) was a bit lower compared to those of the reference Pt/C or the reduced samples (see Fig. 10a and Table 2). The same conclusion is reflected by tabulated mass activity data in Table S3 (Supplementary Materials). Comparable literature results related to ORR investigation on Pt/$Ti_{0.7}Mo_{0.3}O_2$ catalyst [44] attributed the enhancement over the performance of Pt/C to the electronic synergic interaction between Pt and the support, together with the enhanced structural and chemical stability in acidic and oxidative environments provided by the $Ti_{0.7}Mo_{0.3}O_2$ support [45]. XPS investigations described in Sect. 3.2 confirmed the occurrence of electronic metal-support interaction in the presently investigated catalysts. The importance of the synergistic metal–support effect between Mo oxide and Pt to achieve improved ORR catalytic activity was also highlighted in refs. [111,112].

Electrochemical performance of the reference Pt/C, *as-prepared* and reduced $Ti_{0.8}Mo_{0.2}O_2$-C supported Pt electrocatalysts in the HOR by the RDE technique at 900 rpm was compared in Figs. 10c-d. It can be seen from Figs. 10c-d that the potential dynamic polarization curves obtained on these electrocatalysts after 10 cycles of cleaning were very similar, the observed differences being within the expected measurement errors. As shown in Figs. 10c-d, on all catalysts, the current associated with the HOR increases sharply and reaches a limiting plateau at approximately 0.05 V.

This fact is not surprising and is well documented in the literature, indicating that in acid solution on platinum electrodes the rate of hydrogen oxidation reaction is usually too high to measure the difference in activity of different catalysts by RDE [113–115]. Nevertheless, it can be concluded that, regardless of pretreatment, all these catalysts are active in the HOR.

## 4. Discussion

In Section 1.2 a short overview of the main aspects of the metal-support interactions was presented. As it was described in Section 3, several manifestations of these interactions were indeed identified in the present work.

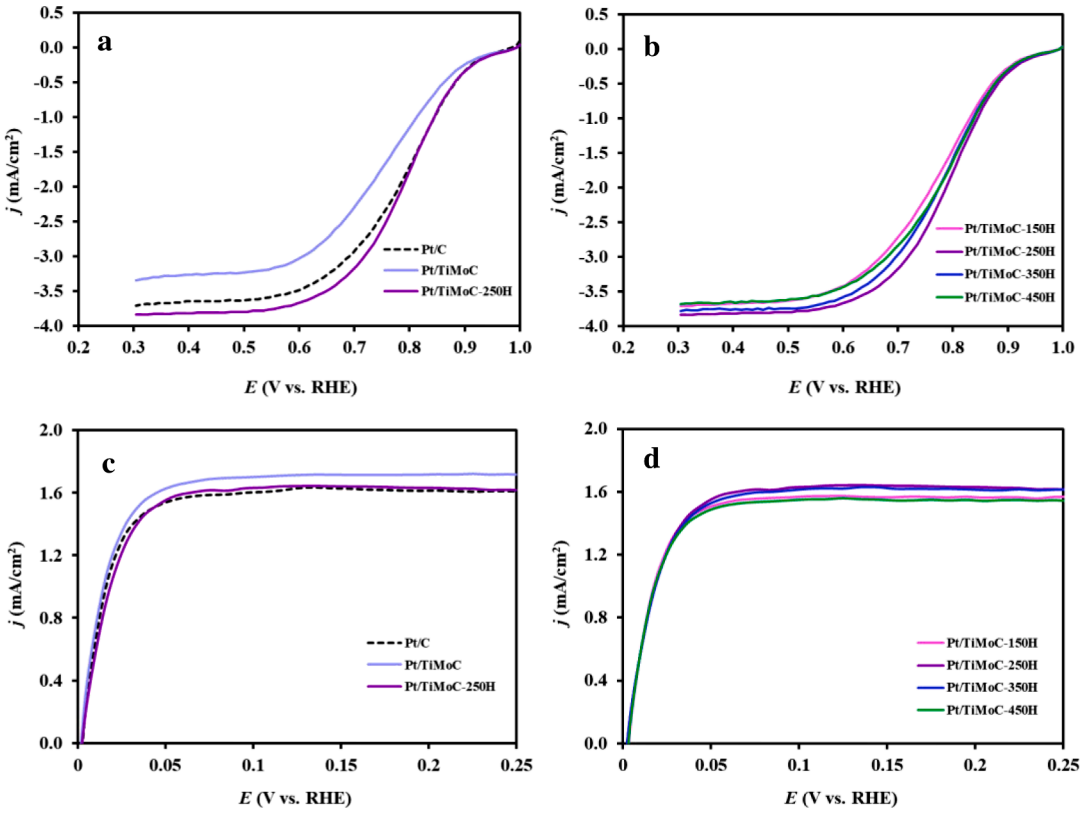


**Fig. 10.** Electrochemical characterization of the reference Pt/C and the Pt/TiMoC catalysts by RDE measurements at 900 rpm: Pt/C (■), *as-prepared* Pt/TiMoC (■) and Pt catalysts reduced at 150 °C (■), 250 °C (■), 350 °C (■) and 450 °C (■). (a, b) ORR curves obtained in $O_2$-saturated 0.5 M $H_2SO_4$; (c, d) HOR curves obtained in a $H_2$-saturated 0.5 M $H_2SO_4$. Recorded at 10 mV $s^{-1}$, T= 25 °C. The currents were normalized to the geometric area of the glassy carbon electrode.

Photoelectron spectroscopy combined with *in situ* hydrogen exposition (Fig. 4) clearly demonstrated appearance of very easily reducible Mo species after the reductive pretreatment, which, as pointed out in our previous work [74], is a convincing sign of the transport of Mo species to the surface of the Pt particles. Although less obvious than in the case of the $Ti_{0.8}Sn_{0.2}O_2$-C composite supported Pt electrocatalyst [70], semi-quantitative analysis of the exposed/buried nature of Pt using the intensity ratio of low and high kinetic energy Pt features also indicated that Pt started to be somewhat buried after reductive pretreatment above 200 °C (Fig. 5), which is consistent with migration of Mo species to its surface during reductive pretreatment in this temperature range. At the same time, the latter result also involves that the decoration layer on Pt is discontinuous or very thin, in contrast with the Pt particles alloyed with tin after reductive pretreatment of the Pt/$Ti_{0.8}Sn_{0.2}O_2$-C system, where relatively thick tin oxide overlayer forms under oxidative conditions [77].

Electrochemical investigations also pointed into the direction of reductive pretreatment-induced material transport. As mentioned above in connection with the bifunctional effect, the prerequisite for easy CO electrooxidation at low potentials (i.e. for enhanced CO tolerance of the electrocatalyst) is the strong coupling of Pt and the oxide. Our previous works, in particular, [88] demonstrated that reducible surface Mo species play a key role in the CO electrooxidation, thus $CO_{ads}$ stripping voltammetry can be regarded as the most sensitive probe of the Pt-Mo coupling among the electrochemical methods used in this work. As described in Sect. 3.3 (in particular, in connection with Fig. 9), reductive pretreatment clearly enhances the CO electrooxidation ability of the electrocatalyst and increases the long-term stability of this feature. This result indicates the enhancement of the Mo-Pt coupling after reductive pretreatment and demonstrates the improved stability of the formed Mo-Pt bifunctional sites. The most plausible explanation for this behavior is the appearance of Mo species on the Pt particles, as concluded from the spectroscopic investigations.

TEM investigations with routine analysis settings, as described in Sect. 3.1, demonstrated the close vicinity of Mo and Pt both in the as prepared electrocatalyst and its reduced counterparts. However, electrochemical studies revealed enhanced Mo-Pt coupling and XPS studies indicated migration of Mo to the surface of the Pt particles, demonstrating that the material transport aspect of the metal-support interaction can indeed be evoked in the Pt/$Ti_{0.8}Mo_{0.2}O_2$-C composite supported electrocatalyst system. At the same time, no evidence was found for encapsulation of the Pt particles by $TiO_x$ or $TiMoO_x$ even at the highest applied pretreatment temperature, which, on the one hand, is a favorable property of the system as encapsulation results in drastic loss of active sites, and, on the other hand, indicates that Mo cations as surface species or as structural defects in the rutile lattice of the mixed oxide are much more mobile than Ti cations as shown schematically in the graphical abstract of this work.

As mentioned above, material transport of SMSI is usually connected to long range interfacial charge transfer. Not surprisingly, this electronic interaction was very frequently observed in catalysts where metal-support interactions are assumed to determine the activity, especially in oxide-supported Pt systems. The typical method of investigation was X-ray absorption spectroscopy, where features around the Pt L-edge can be used to probe the d-band occupancy [44,46]. Core level shifts observed in the Pt XPS spectra can also be used for this purpose [56]. According to data collected in Table S2 of the Supporting Materials, the Pt- and the support-related binding energies (Ti, but also the metal oxide related O 1s component around 530 eV, not shown in Table S2), referenced to the graphitic C 1s peak of the support, showed a clear shift into opposite direction upon even room temperature hydrogen exposure. The decreasing Pt 4f binding energies and the increasing Ti 2p and O 1s

binding energies were consistent with the migration of electrons from the support towards Pt, as expected for these systems. Although it is difficult to judge the extent of charge transfer in the air-exposed (*as-received*) state of the catalysts, in our opinion the described change upon only a slight reduction demonstrates the presence of the electronic interaction in the investigated systems. Nevertheless, it appears that this interaction is invariably present in all catalysts and it is difficult to establish a clear connection between its magnitude and the reductive pretreatment.

Accordingly, the experimental results described in the manuscript clearly demonstrated the development of SMSI in the investigated system, resulting in a clear connection between the improvement of the CO electrooxidation capability of the reduced catalysts and the transfer of Mo species to the Pt particles. Moreover, the slight activity enhancement of the reduced catalysts in the ORR with respect to the *as-prepared* Pt/TiMoC system or the Pt/C reference, as depicted in Fig. 10 or tabulated in the Supplementary Materials (Table S3), can probably also be ascribed to the metal-support interactions. Here, both the co-catalytic effect of the Mo species on Pt and the electronic interaction can contribute to the improved behavior.

As far as the stability of the catalysts is concerned, introduction of the mixed oxide – carbon composite support instead of pure carbon has a clear benefit [66–74], as the oxide provides much stronger binding sites for the Pt particles than the relatively inert carbon surface, or, in other words, the metal-support interaction is much more pronounced in case of the composite support than in pure carbon. One of the most encouraging observations of the present work is that reductive pretreatment can further improve this stabilization effect, which was reflected not only by the lower relative ECSA losses of the reduced catalysts in the long-term stability test, but also by the small changes of the Pt size distribution, especially above the 200–250 °C reduction temperature. Since both the electronic and the material transport aspects of SMSI were present in those reduced catalysts, the most plausible explanation for the better stability is the development of SMSI during the reductive pretreatment. In fact, this reasoning is in line with recent literature results summarized, e.g. in [49,51,78], where SMSI is identified as a way for improving stability of Pt electrocatalysts proposed for fuel cell applications.

## 5. Conclusions

Composites of transitional metal doped $TiO_2$ and carbonaceous materials represent an emerging class of multifunctional supports proposed for Pt electrocatalysts in PEM fuel cells. Beneficial metal-support interactions developing at the Pt-oxide-carbon junctions contribute to higher activity and better stability of the catalysts, which may allow design of effective electrodes with decreased Pt content. Since Pt and the oxide component of the composite support are prone to strong metal-support interaction (SMSI), during which the Pt particles are decorated by partly reduced species originating from the oxide, the focus of the present work is to explore the development of SMSI and its influence on the catalytic performance in these electrocatalysts.

A Pt/$Ti_{0.8}Mo_{0.2}O_2$-C catalyst was prepared using $HNO_3$-glucose-functionalized carbon with mixed oxide/carbon mass ratio of 50/50. Fractions of the *as-prepared* material were subjected to reductive pretreatment in hydrogen at various temperatures in the 150–450 °C range. Structural and surface chemical properties of the resulting catalysts were studied by $N_2$ physisorption, XRD, TEM, STEM-elemental mapping and XPS completed with *in situ* hydrogen exposure experiments. Catalytic functionality was assessed by cyclic voltammetry, $CO_{ads}$ stripping voltammetry and rotating disk electrode measurements in the presence of $H_2$ and $O_2$. Stability was investigated by aging experiments consisting of 500 (short-term) and 10,000 (long-term) potential cycles.

Apart from a limited increase of the size of the Pt particles from 2–3 nm to 4 nm, explained by the competition between Ostwald ripening and the stabilizing effect of the support, structural investigations did not reveal significant differences between the *as-prepared* and the reduced catalysts. Most importantly, elemental maps confirmed the atomic closeness of Pt and the oxide component in all cases, without noticeable change in the spatial distribution of Mo or Ti during the reductive pretreatment. Special XPS investigations, designed to be sensitive for Mo-Pt interactions, however, evidenced transfer of mobile Mo species to the surface of the Pt particles during reductive pretreatment already at 150–250 °C. These Pt-bound Mo species were easily reducible to a metallic surface alloy state upon hydrogen exposure, while became at least partly re-oxidized during air exposure.

Results of the electrochemical investigations were consistent with the surface chemical observations. Features arising from Mo-Pt interactions were detected in the CVs and $CO_{ads}$ stripping voltammograms of both the *as-prepared* catalyst and its reduced counterparts, confirming the excellent low potential CO oxidation ability of all catalysts. However, a more pronounced pre-peak region in the $CO_{ads}$ stripping voltammograms of the reduced samples pointed to a more intimate Mo-Pt coupling in these systems, which can be related to the appearance of Mo species on the surface of the Pt particles. Moreover, the remarkable stability of the pre-peak region during short- and even long-term stability tests was an indicator of the longevity of these Pt-bound Mo species.

The activity of the electrocatalysts in the HOR was not influenced by the appearance of the Mo species on Pt. However, a clear enhancement in the ORR performance was observed in the reduced systems, which, in spite of the ECSA decrease accompanying the pretreatment, became comparable to that of Pt/C, demonstrating the beneficial effect of the closer Mo-Pt coupling on the ORR activity. This result suggested that the mixed oxide-carbon composite supported electrocatalysts, especially after reductive pretreatment, may be useful not only at the anode but also at the cathode electrode of PEMFCs.

Comparison of the long-term stability of the investigated catalysts confirmed the better aging behavior of the *as-prepared* Pt/$Ti_{0.8}Mo_{0.2}O_2$-C with respect to the Pt/C reference. However, even smaller ECSA loss was recorded for the reduced catalysts. On the basis of these studies, reductive pretreatment between 250–350 °C can be recommended for optimizing the properties of Pt/$Ti_{0.8}Mo_{0.2}O_2$-C catalysts by SMSI.

## CRediT authorship contribution statement

**Cristina Silva:** Investigation. **Irina Borbáth:** Writing – review & editing, Writing – original draft, Methodology, Conceptualization. **Erzsébet Dodony:** Investigation. **Dániel Olasz:** Investigation. **György Sáfrán:** Investigation. **Ágnes Szegedi:** Data curation. **Kristóf Zelenka:** Investigation. **András Tompos:** Supervision, Project administration, Funding acquisition. **Zoltán Pászti:** Writing – review & editing, Writing – original draft, Methodology, Investigation, Conceptualization.

## Declaration of competing interest

The authors declare that they have no known competing financial interests or personal relationships that could have appeared to influence the work reported in this paper.

## Data availability

Data will be made available on request.

## Acknowledgements

This research was funded by Project no. RRF-2.3.1-21-2022-00009, titled National Laboratory for Renewable Energy has been implemented with the support provided by the Recovery and Resilience Facility of the European Union within the framework of Programme Széchenyi Plan Plus. Project no. C1792954 has been implemented with

the support provided by the Ministry of Culture and Innovation of Hungary from the National Research, Development and Innovation Fund, financed under the KDP-2021 funding scheme. The support provided by the Hungarian Scientific Research Fund OTKA, Grant number K143216, is also greatly acknowledged.

## Supplementary materials

Supplementary material associated with this article can be found, in the online version, at doi:10.1016/j.materresbull.2024.113114.

## References

[1] E. Kolle-Görgen, G. Fortunato, M. Ledendecker, Catalyst stability in aqueous electrochemistry, Chem. Mater 34 (2022) 10223–10236, https://doi.org/10.1021/acs.chemmater.2c02443.
[2] M.C. Williams, Fuel Cells, in: D.A.B. Dushyant Shekhawat, James J. Spivey (Eds.), Fuel Cells Technol. Fuel Process, Elsevier, 2011, pp. 11–27, https://doi.org/10.1016/B978-0-444-53563-4.10002-1.
[3] J.A. Kent, Handbook of Industrial Chemistry and Biotechnology, Springer International Publishing, USA, 2017, https://doi.org/10.1007/978-3-319-52287-6.
[4] J. Zhang, PEM Fuel Cell Electrocatalysts and Catalyst Layers, 1st ed., Springer London, London, 2008 https://doi.org/10.1007/978-1-84800-936-3.
[5] Z. Chen, D. Higgins, A. Yu, L. Zhang, J. Zhang, A review on non-precious metal electrocatalysts for PEM fuel cells, Energy Environ. Sci. 4 (2011) 3167–3192, https://doi.org/10.1039/c0ee00558d.
[6] J. Zhao, X. Li, A review of polymer electrolyte membrane fuel cell durability for vehicular applications: Degradation modes and experimental techniques, Energy Convers. Manag. 199 (2019) 112022, https://doi.org/10.1016/j.enconman.2019.112022.
[7] J.C. Meier, C. Galeano, I. Katsounaros, A.A. Topalov, A. Kostka, F. Schüth, K.J. J. Mayrhofer, Degradation mechanisms of Pt/C fuel cell catalysts under simulated start–stop conditions, ACS. Catal. 2 (2012) 832–843, https://doi.org/10.1021/cs300024h.
[8] Ş. Neaţu, F. Neaţu, I.M. Chirica, I. Borbáth, E. Tálas, A. Tompos, S. Somacescu, P. Osiceanu, M.A. Folgado, A.M. Chaparro, M. Florea, Recent progress in electrocatalysts and electrodes for portable fuel cells, J. Mater. Chem. A 9 (2021) 17065–17128, https://doi.org/10.1039/D1TA03644K.
[9] V. Stamenkovic, B.S. Mun, K.J.J. Mayrhofer, P.N. Ross, N.M. Markovic, J. Rossmeisl, J. Greeley, J.K. Nørskov, Changing the activity of electrocatalysts for oxygen reduction by tuning the surface electronic structure, Angew. Chemie Int. Ed. 45 (2006) 2897–2901, https://doi.org/10.1002/anie.200504386.
[10] Y.J. Wang, N. Zhao, B. Fang, H. Li, X.T. Bi, H. Wang, Carbon-supported Pt-based alloy electrocatalysts for the oxygen reduction reaction in polymer electrolyte membrane fuel cells: particle size, shape, and composition manipulation and their impact to activity, Chem. Rev. 115 (2015) 3433–3467, https://doi.org/10.1021/cr500519c.
[11] A. Sode, W. Li, Y. Yang, P.C. Wong, E. Gyenge, K.A.R. Mitchell, D. Bizzotto, Electrochemical formation of a Pt/Zn alloy and its use as a catalyst for oxygen reduction reaction in fuel cells, J. Phys. Chem. B 110 (2006) 8715–8722, https://doi.org/10.1021/jp055350s.
[12] G. Samjeské, S. Nagamatsu, S. Takao, K. Nagasawa, Y. Imaizumi, O. Sekizawa, T. Yamamoto, Y. Uemura, T. Uruga, Y. Iwasawa, Performance and characterization of a Pt–Sn (oxidized)/C cathode catalyst with a $SnO_2$-decorated $Pt_3Sn$ nanostructure for oxygen reduction reaction in a polymer electrolyte fuel cell, Phys. Chem. Chem. Phys. 15 (2013) 17208, https://doi.org/10.1039/c3cp52323c.
[13] I. Borbáth, D. Gubán, I. Bakos, Z. Pászti, G. Gajdos, I.E. Sajó, A.Tompos Vass, Exclusive formation of alloy phases via anchoring technique—From bimetallic catalysts to electrocatalysis, Catal. Today 306 (2018) 58–70, https://doi.org/10.1016/j.cattod.2017.01.011.
[14] I. Borbáth, I. Bakos, Z. Pászti, G.P. Szijjártó, A. Tompos, Design of SnPt/C cathode electrocatalysts with optimized Sn/Pt surface composition for potential use in polymer electrolyte membrane fuel cells, Catal. Today 366 (2021) 20–30, https://doi.org/10.1016/j.cattod.2020.06.029.
[15] B.J. Su, K.W. Wang, C.J. Tseng, C.W. Pao, J.L. Chen, K.T. Lu, J.M. Chen, High durability of $Pt_3$ Sn/graphene electrocatalysts toward the oxygen reduction reaction studied with *in situ* QEXAFS, ACS Appl. Mater. Interfaces 12 (2020) 24710–24716, https://doi.org/10.1021/acsami.0c02415.
[16] V.R. Stamenkovic, B.S. Mun, M. Arenz, K.J.J. Mayrhofer, C.A. Lucas, G. Wang, P. N. Ross, N.M. Markovic, Trends in electrocatalysis on extended and nanoscale Pt-bimetallic alloy surfaces, Nat. Mater. 6 (2007) 241–247, https://doi.org/10.1038/nmat1840.
[17] I. Borbáth, D. Gubán, Z. Pászti, I.E. Sajó, E. Drotár, J.L.G. De La Fuente, T. Herranz, S. Rojas, A. Tompos, Controlled synthesis of $Pt_3Sn$/C electrocatalysts with exclusive Sn-Pt interaction designed for use in direct methanol fuel cells, Top. Catal. 56 (2013) 1033–1046, https://doi.org/10.1007/s11244-013-0067-5.
[18] C. Wang, N.M. Markovic, V.R. Stamenkovic, Advanced platinum alloy electrocatalysts for the oxygen reduction reaction, ACS. Catal. 2 (2012) 891–898, https://doi.org/10.1021/cs3000792.
[19] D. Hochfilzer, I. Chorkendorff, J. Kibsgaard, Catalyst stability considerations for electrochemical energy conversion with non-noble metals: do we measure on what we synthesized? ACS. Energy Lett. 8 (2023) 1607–1612, https://doi.org/10.1021/acsenergylett.3c00021.
[20] Z. Liu, J.E. Hu, Q. Wang, K. Gaskell, A.I. Frenkel, G.S. Jackson, B. Eichhorn, PtMo alloy and $MoO_x$@Pt core−shell nanoparticles as highly CO-Tolerant electrocatalysts, J. Am. Chem. Soc. 131 (2009) 6924–6925, https://doi.org/10.1021/ja901303d.
[21] J. Gao, J. Zou, X. Zeng, W. Ding, Carbon supported nano Pt–Mo alloy catalysts for oxygen reduction in magnesium–air batteries, RSC. Adv. 6 (2016) 83025–83030, https://doi.org/10.1039/C6RA16142A.
[22] I. Vernigor, V. Bogdanovskaya, M. Radina, V. Andreev, O. Grafov, PtM/CNT (M = Mo, Ni, CoCr) electrocatalysts with reduced platinum content for anodic hydrogen oxidation and cathodic oxygen reduction in alkaline electrolytes, Catalysts. 13 (2023) 161, https://doi.org/10.3390/catal13010161.
[23] J.M. Jaksic, L. Vracar, S.G. Neophytides, S. Zafeiratos, G. Papakonstantinou, N. V. Krstajic, M.M. Jaksic, Structural effects on kinetic properties for hydrogen electrode reactions and CO tolerance along Mo–Pt phase diagram, Surf. Sci. 598 (2005) 156–173, https://doi.org/10.1016/j.susc.2005.08.036.
[24] B.N. Grgur, N.M. Markovic, P.N. Ross, The electro-oxidation of $H_2$ and $H_2$/CO mixtures on carbon-supported $Pt_x$ $Mo_y$ alloy catalysts, J. Electrochem. Soc. 146 (1999) 1613–1619, https://doi.org/10.1149/1.1391815.
[25] G. Papakonstantinou, F. Paloukis, A. Siokou, S.G. Neophytides, The Electrokinetics of CO Oxidation on $Pt_4$ Mo (20 wt.%) / C Interfaced with Nafion Membrane, J. Electrochem. Soc. 154 (2007) B989, https://doi.org/10.1149/1.2761319.
[26] J.E. Hu, Z. Liu, B.W. Eichhorn, G.S. Jackson, CO tolerance of nano-architectured Pt–Mo anode electrocatalysts for PEM fuel cells, Int. J. Hydrogen Energy 37 (2012) 11268–11275, https://doi.org/10.1016/j.ijhydene.2012.04.094.
[27] S.Y. Huang, P. Ganesan, B.N. Popov, Titania supported platinum catalyst with high electrocatalytic activity and stability for polymer electrolyte membrane fuel cell, Appl. Catal. B Environ. 102 (2011) 71–77, https://doi.org/10.1016/j.apcatb.2010.11.026.
[28] Q. Lv, M. Yin, X. Zhao, C. Li, C. Liu, W. Xing, Promotion effect of $TiO_2$ on catalytic activity and stability of Pt catalyst for electrooxidation of methanol, J. Power Sources 218 (2012) 93–99, https://doi.org/10.1016/j.jpowsour.2012.06.051.
[29] F. Takasaki, S. Matsuie, Y. Takabatake, Z. Noda, A. Hayashi, Y. Shiratori, K. Ito, K. Sasaki, Carbon-Free Pt Electrocatalysts Supported on $SnO_2$ for Polymer Electrolyte Fuel Cells: Electrocatalytic Activity and Durability, J. Electrochem. Soc 158 (2011) B1270–B1275, https://doi.org/10.1149/1.3625918.
[30] H. Zhang, C. Hu, X. He, L. Hong, G. Du, Y. Zhang, Pt support of multidimensional active sites and radial channels formed by $SnO_2$ flower-like crystals for methanol and ethanol oxidation, J. Power Sources 196 (2011) 4499–4505, https://doi.org/10.1016/j.jpowsour.2011.01.030.
[31] R. Samanta, B.K. Manna, R. Trivedi, B. Chakraborty, S. Barman, Hydrogen spillover enhances alkaline hydrogen electrocatalysis on interface-rich metallic Pt-supported $MoO_3$, Chem. Sci. 15 (2024) 364–378, https://doi.org/10.1039/D3SC04126C.
[32] Y. Wang, E.R. Fachini, G. Cruz, Y. Zhu, Y. Ishikawa, J.A. Colucci, C.R. Cabrera, Effect of Surface Composition of Electrochemically Codeposited Platinum/Molybdenum Oxide on Methanol Oxidation, J. Electrochem. Soc. 148 (2001) C222–C226, https://doi.org/10.1149/1.1349881.
[33] J. Shim, C.R. Lee, H.K. Lee, J.S. Lee, E.J. Cairns, Electrochemical characteristics of Pt–$WO_3$/C and Pt–$TiO_2$/C electrocatalysts in a polymer electrolyte fuel cell, J. Power Sources 102 (2001) 172–177, https://doi.org/10.1016/S0378-7753(01)00817-5.
[34] F. Micoud, F. Maillard, A. Bonnefont, N. Job, M. Chatenet, The role of the support in $CO_{ads}$ monolayer electrooxidation on Pt nanoparticles: Pt/$WO_x$ vs. Pt/C, Phys. Chem. Chem. Phys. 12 (2010) 1182–1193, https://doi.org/10.1039/B915244J.
[35] J. Liu, L. Jiang, Electrostatic self-assembly of Pt nanoparticles on hexagonal tungsten oxide as an active CO-tolerant hydrogen oxidation electrocatalyst, Int. J. Hydrogen Energy 43 (2018) 8944–8952, https://doi.org/10.1016/j.ijhydene.2018.03.131.
[36] T.T. Huynh, H.Q. Pham, A. Van Nguyen, S.T. Nguyen, L.G. Bach, V.T.T. Ho, High conductivity and surface area of mesoporous $Ti_{0.7}W_{0.3}O_2$ materials as promising catalyst support for Pt in Proton-Exchange Membrane Fuel Cells, J. Nanosci. Nanotechnol. 19 (2019) 877–881, https://doi.org/10.1166/jnn.2019.15937.
[37] C.V. Subban, Q. Zhou, A. Hu, T.E. Moylan, F.T. Wagner, F.J. Disalvo, Sol-gel synthesis, electrochemical characterization, and stability testing of $Ti_{0.7}W_{0.3}O_2$ nanoparticles for catalyst support applications in proton-exchange membrane fuel cells, J. Am. Chem. Soc. 132 (2010) 17531–17536, https://doi.org/10.1021/ja1074163.
[38] B.J. Hsieh, M.C. Tsai, C.J. Pan, W.N. Su, J. Rick, J.F. Lee, Y.W. Yang, B.J. Hwang, Platinum loaded on dual-doped $TiO_2$ as an active and durable oxygen reduction reaction catalyst, NPG. Asia Mater. 9 (2017), https://doi.org/10.1038/am.2017.78.
[39] K.W. Park, K.S. Seol, Nb-$TiO_2$ supported Pt cathode catalyst for polymer electrolyte membrane fuel cells, Electrochem. Commun. 9 (2007) 2256–2260, https://doi.org/10.1016/j.elecom.2007.06.027.
[40] S.Y. Huang, P. Ganesan, B.N. Popov, Electrocatalytic activity and stability of niobium-doped titanium oxide supported platinum catalyst for polymer electrolyte membrane fuel cells, Appl. Catal. B Environ. 96 (2010) 224–231, https://doi.org/10.1016/j.apcatb.2010.02.025.
[41] S. Shahgaldi, J. Hamelin, The effect of low platinum loading on the efficiency of PEMFC's electrocatalysts supported on $TiO_2$–Nb, and $SnO_2$–Nb: An experimental

comparison between active and stable conditions, Energy Convers. Manag. 103 (2015) 681–690, https://doi.org/10.1016/J.ENCONMAN.2015.06.050.
[42] J.H. Kim, G. Kwon, H. Lim, C. Zhu, H. You, Y.T. Kim, Effects of transition metal doping in Pt/M-$TiO_2$ (M = V, Cr, and Nb) on oxygen reduction reaction activity, J. Power Sources 320 (2016) 188–195, https://doi.org/10.1016/j.jpowsour.2016.04.019.
[43] T. Arashi, J. Seo, K. Takanabe, J. Kubota, K. Domen, Nb-doped $TiO_2$ cathode catalysts for oxygen reduction reaction of polymer electrolyte fuel cells, Catal. Today 233 (2014) 181–186, https://doi.org/10.1016/J.CATTOD.2013.12.009.
[44] V.T.T. Ho, C.J. Pan, J. Rick, W.N. Su, B.J. Hwang, Nanostructured $Ti_{0.7}Mo_{0.3}O_2$ support enhances electron transfer to Pt: high-performance catalyst for oxygen reduction reaction, J. Am. Chem. Soc. 133 (2011) 11716–11724, https://doi.org/10.1021/ja2039562.
[45] T.T. Nguyen, V.T.T. Ho, C.J. Pan, J.Y. Liu, H.L. Chou, J. Rick, W.N. Su, B. J. Hwang, Synthesis of $Ti_{0.7}Mo_{0.3}O_2$ supported-Pt nanodendrites and their catalytic activity and stability for oxygen reduction reaction, Appl. Catal. B Environ. 154–155 (2014) 183–189, https://doi.org/10.1016/j.apcatb.2014.02.018.
[46] M.C. Tsai, T.T. Nguyen, N.G. Akalework, C.J. Pan, J. Rick, Y.F. Liao, W.N. Su, B. J. Hwang, Interplay between molybdenum dopant and oxygen vacancies in a $TiO_2$ support enhances the Oxygen Reduction Reaction, ACS. Catal. 6 (2016) 6551–6559, https://doi.org/10.1021/acscatal.6b00600.
[47] Y. Gao, M. Hou, Z. Shao, C. Zhang, X. Qin, B. Yi, Preparation and characterization of $Ti_{0.7}Sn_{0.3}O_2$ as catalyst support for oxygen reduction reaction, J. Energy Chem. 23 (2014) 331–337, https://doi.org/10.1016/S2095-4956(14)60155-8.
[48] A. Sengele, D. Robert, N. Keller, C. Colbeau-Justin, V. Keller, Sn-doped and porogen-modified $TiO_2$ photocatalyst for solar light elimination of sulfure diethyle as a model for chemical warfare agent, Appl. Catal. B Environ. 245 (2019) 279–289, https://doi.org/10.1016/J.APCATB.2018.12.071.
[49] C.J. Pan, M.C. Tsai, W.N. Su, J. Rick, N.G. Akalework, A.K. Agegnehu, S.Y. Cheng, B.J. Hwang, Tuning/exploiting strong metal-support interaction (SMSI) in heterogeneous catalysis, J. Taiwan Inst. Chem. Eng. 74 (2017) 154–186, https://doi.org/10.1016/j.jtice.2017.02.012.
[50] Q. Fu, T. Wagner, Interaction of nanostructured metal overlayers with oxide surfaces, Surf. Sci. Rep. 62 (2007) 431–498, https://doi.org/10.1016/j.surfrep.2007.07.001.
[51] M. Chen, R. Peng, M. Zhengpei, L. Junming, L. Jing, D. Peilin, H. Wei, T. Xinlong, Strong metal-support interaction of Pt-based electrocatalysts with transition metal oxides/nitrides/carbides for oxygen reduction reaction, Microstructures 3 (2023) 2023025, https://doi.org/10.20517/microstructures.2023.12.
[52] B.J. Hsieh, M.C. Tsai, C.J. Pan, W.N. Su, J. Rick, H.L. Chou, J.F. Lee, B.J. Hwang, Tuning metal support interactions enhances the activity and durability of $TiO_2$-supported Pt nanocatalysts, Electrochim. Acta 224 (2017) 452–459, https://doi.org/10.1016/j.electacta.2016.12.020.
[53] H.O. Otor, J.B. Steiner, C. García-Sancho, A.C. Alba-Rubio, Encapsulation methods for control of catalyst deactivation: a review, ACS. Catal. 10 (2020) 7630–7656, https://doi.org/10.1021/acscatal.0c01569.
[54] X.Q. Cao, J. Zhou, S. Li, G.W. Qin, Ultra-stable metal nano-catalyst synthesis strategy: a perspective, Rare Met 39 (2020) 113–130, https://doi.org/10.1007/s12598-019-01350-y.
[55] I. Jiménez-Morales, S. Cavaliere, D. Jones, J. Rozière, Strong metal-support interaction improves activity and stability of Pt electrocatalysts on doped metal oxides, Phys. Chem. Chem. Phys. 20 (2018) 8765–8772, https://doi.org/10.1039/c8cp00176f.
[56] W. Shi, A.H. Park, Z. Li, S. Xu, J.M. Kim, P.J. Yoo, Y.U. Kwon, Sub-nanometer thin $TiO_2$-coating on carbon support for boosting oxygen reduction activity and durability of Pt nanoparticles, Electrochim, Acta 394 (2021) 139127, https://doi.org/10.1016/j.electacta.2021.139127.
[57] J. Wang, M. Xu, J. Zhao, H. Fang, Q. Huang, W. Xiao, T. Li, D. Wang, Anchoring ultrafine Pt electrocatalysts on $TiO_2$-C via photochemical strategy to enhance the stability and efficiency for oxygen reduction reaction, Appl. Catal. B Environ. 237 (2018) 228–236, https://doi.org/10.1016/j.apcatb.2018.05.085.
[58] I. Gatto, A. Saccà, R. Pedicini, E. Passalacqua, A. Carbone, Evaluation of titanium oxide introduction in the electrode structure for portable PEMFC applications, Int. J. Hydrogen Energy 46 (2021) 27687–27699, https://doi.org/10.1016/j.ijhydene.2021.05.200.
[59] S. von Kraemer, K. Wikander, G. Lindbergh, A. Lundblad, A.E.C. Palmqvist, Evaluation of $TiO_2$ as catalyst support in Pt-$TiO_2$/C composite cathodes for the proton exchange membrane fuel cell, J. Power Sources 180 (2008) 185–190, https://doi.org/10.1016/j.jpowsour.2008.02.023.
[60] W. Vogel, L. Timperman, N. Alonso-Vante, Probing metal substrate interaction of Pt nanoparticles: Structural XRD analysis and oxygen reduction reaction, Appl. Catal. A Gen. 377 (2010) 167–173, https://doi.org/10.1016/j.apcata.2010.01.034.
[61] X.L. Sui, Z.B. Wang, M. Yang, L. Huo, D.M. Gu, G.P. Yin, Investigation on C–$TiO_2$ nanotubes composite as Pt catalyst support for methanol electrooxidation, J. Power Sources 255 (2014) 43–51, https://doi.org/10.1016/j.jpowsour.2014.01.001.
[62] Y. Jin, D. Han, W. Jia, F. Li, X. Chen, G. Huang, D. Zhang, $WO_3$ modified graphene supported Pt electrocatalysts with enhanced performance for oxygen reduction reaction, Int. J. Electrochem. Sci. 12 (2017) 6535–6544, https://doi.org/10.20964/2017.07.32.
[63] Y. Li, C. Liu, Y. Liu, B. Feng, L. Li, H. Pan, W. Kellogg, D. Higgins, G. Wu, Sn-doped $TiO_2$ modified carbon to support Pt anode catalysts for direct methanol fuel cells, J. Power Sources 286 (2015) 354–361, https://doi.org/10.1016/j.jpowsour.2015.03.155.
[64] A. Ignaszak, C. Song, W. Zhu, Y.J. Wang, J. Zhang, A. Bauer, R. Baker, V. Neburchilov, S. Ye, S. Campbell, Carbon–$Nb_{0.07}Ti_{0.93}O_2$ composite supported Pt–Pd electrocatalysts for PEM fuel cell oxygen reduction reaction, Electrochim. Acta 75 (2012) 220–228, https://doi.org/10.1016/J.ELECTACTA.2012.04.111.
[65] H.T.Q. Pham, H.Q. Pham, Q. Huynh, T.N. Nguyen, N.H.T. Huynh, T.Q. Nguyen, T. T. Huynh, Synthesis and characterization of $Ti_{0.9}Ir_{0.1}O_2$-activated carbon composite as a promising support for catalysts in electrochemical energy conversion, Adv. Nat. Sci. Nanosci. Nanotechnol. 14 (2023) 35003, https://doi.org/10.1088/2043-6262/ace432.
[66] I. Ayyubov, E. Tálas, I. Borbáth, Z. Pászti, C. Silva, Á. Szegedi, A. Kuncser, M. S. Yazici, I.E. Sajó, T. Szabó, A. Tompos, Composites of titanium–molybdenum mixed oxides and non-traditional carbon materials: innovative supports for platinum electrocatalysts for polymer electrolyte membrane fuel cells, Nanomaterials 14 (2024) 1053, https://doi.org/10.3390/nano14121053.
[67] Á. Vass, I. Borbáth, I. Bakos, Z. Pászti, G. Sáfrán, A. Tompos, Stability issues of CO tolerant Pt-based electrocatalysts for polymer electrolyte membrane fuel cells: comparison of Pt/$Ti_{0.8}Mo_{0.2}O_2$–C with PtRu/C, React. Kinet. Mech. Catal. 126 (2019) 679–699, https://doi.org/10.1007/s11144-018-1512-z.
[68] I. Borbáth, K. Zelenka, Á. Vass, Z. Pászti, G.P. Szijjártó, Z. Sebestyén, G. Sáfrán, A. Tompos, CO tolerant Pt electrocatalysts for PEM fuel cells with enhanced stability against electrocorrosion, Int. J. Hydrogen Energy 46 (2021) 13534–13547, https://doi.org/10.1016/j.ijhydene.2020.08.002.
[69] I. Borbáth, E. Tálas, Z. Pászti, K. Zelenka, I. Ayyubov, K. Salmanzade, I.E. Sajó, G. Sáfrán, A. Tompos, Investigation of Ti-Mo mixed oxide-carbon composite supported Pt electrocatalysts: Effect of the type of carbonaceous materials, Appl. Catal. A Gen. (2021) 620, https://doi.org/10.1016/j.apcata.2021.118155.
[70] C. Silva, K. Salmanzade, I. Borbáth, E. Dódony, D. Olasz, G. Sáfrán, A. Kuncser, E. Pászti-Gere, A. Tompos, Z. Pászti, Reductive treatment of Pt supported on $Ti_{0.8}Sn_{0.2}O_2$-C composite: a route for modulating the Sn–Pt interactions, Nanomaterials 13 (2023), https://doi.org/10.3390/nano13152245.
[71] D. Gubán, I. Borbáth, Z. Pászti, I. Sajó, E. Drotár, M. Hegedus, A. Tompos, Preparation and characterization of novel $Ti_{0.7}W_{0.3}O_2$-C composite materials for Pt-based anode electrocatalysts with enhanced CO tolerance, Appl. Catal. B Environ. 174–175 (2015) 455–470, https://doi.org/10.1016/j.apcatb.2015.03.031.
[72] D. Gubán, A. Tompos, I. Bakos, Z.Pászti Vass, E.G. Szabó, I.E. Sajó, I. Borbáth, Preparation of CO-tolerant anode electrocatalysts for polymer electrolyte membrane fuel cells, Int. J. Hydrogen Energy 42 (2017) 13741–13753, https://doi.org/10.1016/j.ijhydene.2017.03.080.
[73] M.S. Yazici, S. Dursun, I. Borbáth, A. Tompos, Reformate gas composition and pressure effect on CO tolerant Pt/$Ti_{0.8}Mo_{0.2}O_2$–C electrocatalyst for PEM fuel cells, Int. J. Hydrogen Energy 46 (2021) 13524–13533, https://doi.org/10.1016/j.ijhydene.2020.08.226.
[74] D. Diczházi, I. Borbáth, I. Bakos, G.P. Szijjártó, A. Tompos, Z. Pászti, Design of Mo-doped mixed oxide–carbon composite supports for Pt-based electrocatalysts: the nature of the Mo-Pt interaction, Catal. Today 366 (2021) 31–40, https://doi.org/10.1016/j.cattod.2020.04.004.
[75] C. Silva, I. Borbáth, K. Zelenka, I.E. Sajó, G. Sáfrán, A. Tompos, Z. Pászti, Effect of the reductive treatment on the state and electrocatalytic behavior of Pt in catalysts supported on $Ti_{0.8}Mo_{0.2}O_2$-C composite, React. Kinet. Mech. Catal. 135 (2022) 29–47, https://doi.org/10.1007/s11144-021-02131-4.
[76] T. Daio, A. Staykov, L. Guo, J. Liu, M. Tanaka, S.Matthew Lyth, K. Sasaki, Lattice Strain Mapping of Platinum Nanoparticles on Carbon and $SnO_2$ Supports, Sci. Rep. 5 (2015) 13126, https://doi.org/10.1038/srep13126.
[77] M. Batzill, U. Diebold, The surface and materials science of tin oxide, Prog. Surf. Sci. 79 (2005) 47–154, https://doi.org/10.1016/j.progsurf.2005.09.002.
[78] F. Qi, J. Peng, Z. Liang, J. Guo, J. Liu, T. Fang, H. Mao, Strong metal-support interaction (SMSI) in environmental catalysis: Mechanisms, application, regulation strategies, and breakthroughs, Environ. Sci. Ecotechnology 22 (2024) 100443, https://doi.org/10.1016/j.ese.2024.100443.
[79] J.C. Matsubu, S. Zhang, L. DeRita, N.S. Marinkovic, J.G. Chen, G.W. Graham, X. Pan, P. Christopher, Adsorbate-mediated strong metal-support interactions in oxide-supported Rh catalysts, Nat. Chem. 9 (2017) 120–127, https://doi.org/10.1038/NCHEM.2607.
[80] X. Liu, M.H. Liu, Y.C. Luo, C.Y. Mou, S.D. Lin, H. Cheng, J.M. Chen, J.F. Lee, T. S. Lin, Strong Metal–support interactions between gold nanoparticles and ZnO nanorods in CO oxidation, J. Am. Chem. Soc. 134 (2012) 10251–10258, https://doi.org/10.1021/ja3033235.
[81] J. Dong, Q. Fu, Z. Jiang, B. Mei, X. Bao, Carbide-supported au catalysts for water–gas shift reactions: a new territory for the strong metal–support interaction effect, J. Am. Chem. Soc. 140 (2018) 13808–13816, https://doi.org/10.1021/jacs.8b08246.
[82] J. Dong, Q. Fu, H. Li, J. Xiao, B. Yang, B. Zhang, Y. Bai, T. Song, R. Zhang, L. Gao, J. Cai, H. Zhang, Z. Liu, X. Bao, Reaction-induced strong metal–support interactions between metals and inert boron nitride nanosheets, J. Am. Chem. Soc. 142 (2020) 17167–17174, https://doi.org/10.1021/jacs.0c08139.
[83] H. Wang, L. Wang, D. Lin, X. Feng, Y. Niu, B. Zhang, F.S. Xiao, Strong metal–support interactions on gold nanoparticle catalysts achieved through Le Chatelier's principle, Nat. Catal. 4 (2021) 418–424, https://doi.org/10.1038/s41929-021-00611-3.
[84] W.S. Rasband, ImageJ, Natl. Institutes Heal. Bethesda, Maryland, USA (n.d.). https://imagej.nih.gov/ij/.
[85] N. Fairley, CasaXPS: Spectrum processing software for XPS, AES and SIMS, Cheshiree (2006).
[86] M. Mohai, XPS MultiQuant, Multimodel XPS quantification software, Surf. Interface Anal. 36 (2004) 828–832, https://doi.org/10.1002/sia.1775.

[87] M. Mohai, XPS MultiQuant, Multi-model X-ray photoelectron spectroscopy quantification program, Version 7.00.92 (2011).
[88] A. Vass, I. Borbáth, I. Bakos, Z. Pászti, I.E. Sajó, A. Tompos, Novel Pt electrocatalysts: multifunctional composite supports for enhanced corrosion resistance and improved CO tolerance, Top. Catal. 61 (2018) 1300–1312, https://doi.org/10.1007/s11244-018-0988-0.
[89] J. Baltrusaitis, B. Mendoza-Sanchez, V. Fernandez, R. Veenstra, N. Dukstiene, A. Roberts, N. Fairley, Generalized molybdenum oxide surface chemical state XPS determination via informed amorphous sample model, Appl. Surf. Sci. 326 (2015) 151–161, https://doi.org/10.1016/j.apsusc.2014.11.077.
[90] T. Schroeder, J. Zegenhagen, N. Magg, B. Immaraporn, H.J. Freund, Formation of a faceted $MoO_2$ epilayer on Mo (112) studied by XPS, UPS and STM, Surf. Sci. 552 (2004) 85–97, https://doi.org/10.1016/j.susc.2004.01.010.
[91] D.O. Scanlon, G.W. Watson, D.J. Payne, G.R. Atkinson, R.G. Egdell, D.S.L. Law, Theoretical and experimental study of the electronic structures of $MoO_3$ and $MoO_2$, J. Phys. Chem. C 114 (2010) 4636–4645, https://doi.org/10.1021/jp9093172.
[92] S. Somacescu, P. Osiceanu, J.M. Calderon Moreno, D.C. Culita, F. Neațu, M. M. Trandafir, Ș. Neațu, A. Kuncser, G.P. Szijjártó, E. Tálas, A. Tompos, I. Borbáth, M. Florea, Design of electrocatalysts with reduced Pt content supported on mesoporous $NiWO_4$ and $NiWO_4$-graphene nanoplatelets composite for oxygen reduction and hydrogen oxidation in acidic medium, Int. J. Hydrogen Energy 48 (2023) 6317–6335, https://doi.org/10.1016/j.ijhydene.2022.04.270.
[93] I. Ayyubov, E. Tálas, K. Salmanzade, A. Kuncser, Z. Pászti, Ștefan Neațu, A. G. Mirea, M. Florea, A. Tompos, I. Borbáth, Electrocatalytic properties of mixed-oxide-containing composite-supported platinum for polymer electrolyte membrane (PEM) fuel cells, Materials. (Basel) 15 (2022) 3671, https://doi.org/10.3390/ma15103671.
[94] R. Woods, Electroanalytical Chemistry: A Series of Advances: Volume 9, 9th ed., Dekker Marcel Inc, New York, 1976, pp. 1–162, in: A.J. Bard (Ed.).
[95] Á. Vass, I. Borbáth, Z. Pászti, I. Bakos, I.E. Sajó, P. Németh, A. Tompos, Effect of Mo incorporation on the electrocatalytic performance of Ti–Mo mixed oxide–carbon composite supported Pt electrocatalysts, React. Kinet. Mech. Catal. 121 (2017) 141–160, https://doi.org/10.1007/s11144-017-1155-5.
[96] N.R. Elezović, L.M. Gajić-Krstajić, L.M. Vračar, N.V. Krstajić, Effect of chemisorbed CO on $MoO_x$–Pt/C electrode on the kinetics of hydrogen oxidation reaction, Int. J. Hydrogen Energy 35 (2010) 12878–12887, https://doi.org/10.1016/j.ijhydene.2010.09.004.
[97] M. Hakamizadeh, S. Afshar, A. Tadjarodi, R. Khajavian, M.R. Fadaie, B. Bozorgi, Improving hydrogen production via water splitting over Pt/$TiO_2$/activated carbon nanocomposite, Int. J. Hydrogen Energy 39 (2014) 7262–7269, https://doi.org/10.1016/j.ijhydene.2014.03.048.
[98] C. Odetola, L.N. Trevani, E.B. Easton, Photo enhanced methanol electrooxidation: Further insights into Pt and $TiO_2$ nanoparticle contributions, Appl. Catal. B Environ. 210 (2017) 263–275, https://doi.org/10.1016/j.apcatb.2017.03.027.
[99] C. Odetola, L. Trevani, E.B. Easton, Enhanced activity and stability of Pt/$TiO_2$/carbon fuel cell electrocatalyst prepared using a glucose modifier, J. Power Sources 294 (2015) 254–263, https://doi.org/10.1016/j.jpowsour.2015.06.066.
[100] C. Odetola, E.B. Easton, L. Trevani, Investigation of $TiO_2$/carbon electrocatalyst supports prepared using glucose as a modifier, Int. J. Hydrogen Energy 41 (2016) 8199–8208, https://doi.org/10.1016/j.ijhydene.2015.10.035.
[101] S. Feng, J. Lu, L. Luo, G. Qian, J. Chen, H.S. Abbo, S.J.J. Titinchi, S. Yin, Enhancement of oxygen reduction activity and stability via introducing acid-resistant refractory Mo and regulating the near-surface Pt content, J. Energy Chem. 51 (2020) 246–252, https://doi.org/10.1016/J.JECHEM.2020.03.063.
[102] Z. Zhang, J. Liu, J. Gu, L. Su, L. Cheng, An overview of metal oxide materials as electrocatalysts and supports for polymer electrolyte fuel cells, Energy Environ. Sci. 7 (2014) 2535–2558, https://doi.org/10.1039/c3ee43886d.
[103] L. Guczi, A. Erdöhelyi, Catalysis for Alternative Energy Generation, Springer New York, New York, NY, 2012, https://doi.org/10.1007/978-1-4614-0344-9.
[104] O. Guillén-Villafuerte, G. García, J.L. Rodríguez, E. Pastor, R. Guil-López, E. Nieto, J.L.G. Fierro, Preliminary studies of the electrochemical performance of Pt/X@$MoO_3$/C (X = $Mo_2C$, $MoO_2$, $Mo^0$) catalysts for the anode of a DMFC: Influence of the Pt loading and Mo-phase, Int. J. Hydrogen Energy 38 (2013) 7811–7821, https://doi.org/10.1016/j.ijhydene.2013.04.083.
[105] G. Samjeské, H. Wang, T. Löffler, H. Baltruschat, CO and methanol oxidation at Pt-electrodes modified by Mo, Electrochim. Acta 47 (2002) 3681–3692, https://doi.org/10.1016/S0013-4686(02)00338-9.
[106] I. Bakos, I. Borbáth, Á. Vass, Z. Pászti, A. Tompos, Design and investigation of molybdenum modified platinum surfaces for modeling of CO tolerant electrocatalysts, Top. Catal. 61 (2018) 1385–1395, https://doi.org/10.1007/s11244-018-1035-x.
[107] E.M. Crabb, M.K. Ravikumar, Y. Qian, A.E. Russell, S. Maniguet, J. Yao, D. Thompsett, M. Hurford, S.C. Ball, Controlled modification of carbon supported platinum electrocatalysts by Mo, Electrochem. Solid-State Lett. 5 (2002) A5–A9, https://doi.org/10.1149/1.1419703.
[108] R.A.M. Esfahani, S.K. Vankova, A.H.A. Monteverde Videla, S. Specchia, Innovative carbon-free low content Pt catalyst supported on Mo-doped titanium suboxide ($Ti_3O_5$-Mo) for stable and durable oxygen reduction reaction, Appl. Catal. B Environ. 201 (2017) 419–429, https://doi.org/10.1016/j.apcatb.2016.08.041.
[109] G. Alkan, V.P.M. Košević, M. Mihailović, S. Stopic, B. Friedrich, J. Stevanović, V. Panić, Characterization of defined pt particles prepared by ultrasonic spray pyrolysis for one-step synthesis of supported ORR composite catalysts, Metals. (Basel) 12 (2) (2022) 290, https://doi.org/10.3390/met12020290.
[110] K.J.J. Mayrhofer, D. Strmcnik, B.B. Blizanac, V. Stamenkovic, M. Arenz, N. M. Markovic, Measurement of oxygen reduction activities via the rotating disc electrode method: From Pt model surfaces to carbon-supported high surface area catalysts, Electrochim. Acta 53 (2008) 3181–3188, https://doi.org/10.1016/j.electacta.2007.11.057.
[111] Z. Yan, J. Xie, J. Jing, M. Zhang, W. Wei, S. Yin, $MoO_2$ nanocrystals down to 5 nm as Pt electrocatalyst promoter for stable oxygen reduction reaction, Int. J. Hydrogen Energy 37 (2012) 15948–15955, https://doi.org/10.1016/j.ijhydene.2012.08.033.
[112] P.F.B.D. Martins, E.A. Ticianelli, Electrocatalytic activity and stability of platinum nanoparticles supported on carbon-molybdenum oxides for the oxygen reduction reaction, ChemElectroChem. 2 (2015) 1298–1306, https://doi.org/10.1002/celc.201500196.
[113] W. Sheng, H.A. Gasteiger, Y. Shao-Horn, Hydrogen oxidation and evolution reaction kinetics on platinum: acid vs alkaline electrolytes, J. Electrochem. Soc 157 (2010) B1529–B1536, https://doi.org/10.1149/1.3483106.
[114] K.C. Neyerlin, W. Gu, J. Jorne, H.A. Gasteiger, Study of the exchange current density for the hydrogen oxidation and evolution reactions, J. Electrochem. Soc. 154 (2007) B631–B635, https://doi.org/10.1149/1.2733987.
[115] C.M. Zalitis, J. Sharman, E. Wright, A.R. Kucernak, Properties of the hydrogen oxidation reaction on Pt/C catalysts at optimised high mass transport conditions and its relevance to the anode reaction in PEFCs and cathode reactions in electrolysers, Electrochim. Acta 176 (2015) 763–776, https://doi.org/10.1016/j.electacta.2015.06.146.